



Budget of the total nitrogen in the Yucatan Shelf: driving mechanisms through a physical-biogeochemical coupled model

Sheila N. Estrada-Allis¹, Joao M. Azevedo Correia de Souza², Julio Sheinbaum Pardo¹, Cecilia Henriquez Ortiz³, Ismael Mariño Tapia³, and Jorge A. Herrera-Silveira³

¹Physical Oceanography Department, CICESE, Ensenada, Baja California, Mexico

²MetOcean Solutions / MetService. Raglan. New Zealand.

³Departamento Recursos del Mar, CINVESTAV, Merida, Yucatan, Mexico.

Correspondence: Sheila N. Estrada-Allis (sheila@cicese.mx)

Abstract. Continental shelves are the most productive areas in the seas with strongest implications for global Total Nitrogen (TN) cycling. The Yucatan shelf is the largest shelf in the Gulf of Mexico (GoM), however, its general TN budget has not been quantified. This is largely due to the lack of significant spatio-temporal *in situ* measurements and the complexity of the shelf dynamics, including the Yucatan Current, coastal upwelling, Coastal Trapped Waves (CTWs) and bottom Ekman transport.

5 Through a nine years output of a coupled physical-biogeochemical model of the GoM, the TN budget in the Yucatan shelf is quantified. Results indicate that the main entrance of inorganic nitrogen is through its southern and eastern margins. The TN is then advected to the oligotrophic deep GoM and to the deep Campeche bay. The analysis also shows that the inner shelf (50 m isobath) is efficient in terms of TN, since all the DIN imported into the shelf is consumed by the phytoplankton. Rivers contribute 20 % of the TN, while denitrification removes up to 53 % of TN that enters into the inner shelf. The high-
10 frequency variability of the TN fluxes are modulated by the Yucatan Current in the south and by bottom Ekman transport produced by this current against the shelf-break (250 m isobath) in the east. This current-topography interaction can help to maintain the upwelling of Cape Catoche, uplifting nutrient-rich water into the euphotic layer. The export of TN at both western and northwestern margins is modulated by CTWs with a mean period of 10 days in agreement with recent observational and modelling studies.

15 1 Introduction

Continental shelves are the most productive areas in the ocean, widely recognized to play a critical role in the global cycling of nitrogen and carbon (e.g., Fennel, 2010; Liu et al., 2010). The importance of continental shelves also lies in its direct implications for human activities, such as fisheries, tourism, and resources. Their interaction with anthropogenic pollution sources is hence expected to have significant consequences not only in socio-economical activities, e.g., overfishing, acidifi-
20 cation, eutrophication (Enriquez et al., 2010), but also in the climate system, e.g., hypoxia/anoxia zones, pCO₂ and sediment denitrification (Fennel et al., 2006; Seitzinger et al., 2006).

Nutrient fluxes are intrinsically related with the productivity and nitrogen cycling of the shelves. However, sources and sinks of nutrients are highly uncertain and difficult to quantify. This is partly due to the large spatial and temporal variability



associated with the cross-shelf and along-shelf regional nutrient budgets and the difficulty to measure them. Biogeochemical coupled modeling systems are a useful tool to quantify the shelf-open ocean nutrient exchange, taking into account the different spatial and temporal scales implicated in the biogeochemical cycle (Fennel et al., 2006; Hermann et al., 2009; Xue et al., 2013; Damien et al., 2018).

5 The physical mechanisms that drive and modulate the cross-shelf transport of nutrients and biogenic material are also poorly known. Shelves are rich dynamical areas in which several process can coexist at different spatio-temporal scales. Ekman divergence, CTWs, current interactions with the shelf break, mesoscale structures, vertical mixing and topographic interactions, among others, are recurrent processes that may uplift nutrient-rich waters from the deep ocean into the photic zone in the shelves (e.g., Cochrane, 1966; Merino, 1997; Roughan and Middleton, 2002, 2004; Hermann et al., 2009; Shaeffer et al., 2014; 10 Jouanno et al., 2018).

In this study, we use a coupled physical-biogeochemical model to study the nitrogen budget in the Yucatan Shelf (YS), which is the largest continental shelf in the Gulf of Mexico (GoM, Figure 1). The biological cycling of the YS is one the most poorly known processes in the GoM and controversies remain regarding its physical dynamics besides the long-term undersampling of biogeochemical variables (Zavala-Hidalgo et al., 2014; Damien et al., 2018), and the presence of underground freshwater 15 discharges with unknown fluxes. The main objectives of this study include: (i) the quantification of the Total Nitrogen (TN) budget within the inner and outer YS; (ii) examine the sources and sinks of nitrogen in the continental shelf and (iii) analyze the physical mechanisms that modulate the cross-shelf TN transport.

1.1 The study area: Yucatan shelf

20 With a horizontal extension of almost 250 km, the YS or Campeche Bank (Figure 1b and c) is one of the largest shelves in the world. The wind pattern over the YS is mainly influenced by the trade winds (easterly winds) throughout the year, with sporadic northeasterly wind events caused by cold fronts with relatively short duration (Gutierrez-de Velasco and Winant, 1996; Enriquez et al., 2013). These easterly winds drive a westward circulation over the shelf (Enriquez et al., 2010; Ruiz-Castillo et al., 2016).

The YS is a highly dynamic region due to the coexistence of different physical processes. Merino (1997) reported the uplift 25 of Caribbean waters from 220-250 m deep, reaching the YS at the “notch area” (small black box in Figure 1). This happens due to the interaction of the Yucatan Current with the slope of the YS on its eastern side (Cochrane, 1966; Merino, 1997; Ochoa et al., 2001; Sheinbaum et al., 2002) which favors the outcrop of deep nutrient-rich waters to shallower layers over the shelf. However, the mechanisms responsible of the upwelling remains unclear.

The alongshore westward winds are also responsible for upwelling events due to divergent Ekman transport at Cape Catoche 30 (Figure 2). The upwelling is suggested to be present year-round along the north and northeast coast of the YS, with intensifications during spring and autumn (Zavala-Hidalgo et al., 2006). This pattern is corroborated by the model as shown in Figure 2. However, there are controversies regarding the seasonality of the upwelling. Observational studies show that the upwelled waters usually cannot reach the photic layer (Merino, 1997; Enriquez et al., 2013). Therefore, it is expected that the variability of the upwelling can be influenced by the dynamics of the Yucatan Current (Sheinbaum et al., 2002) and by the wind-driven



Ekman transport (Enriquez et al., 2010; Reyes-Mendoza et al., 2016). Dynamical processes that may also be important for the upwelling include the extension and the intensity of the Loop Current (Bunge et al., 2002; Jouanno et al., 2018), CTWs (Jouanno et al., 2016), and the bottom Ekman transport. External (off-shelf) sea level may also generate pressure gradients that oppose the upwelling and explain its seasonality.

5 Regarding the freshwater inflow, a significant amount of sources have been identified in the YS related to groundwater inflows due to the karstic geological formation of Yucatan peninsula (Pope et al., 1191; Gallardo and Marui, 2006), coastal lagoons (Herrera-Silveira et al., 2004), and sinkholes. Due to the complexity of processes and scarcity of observations, the total discharge of freshwater into the YS is not well known.

Owing to the spatial and temporal scarcity of biogeochemical observations, the budget and pathways of nitrogen to the GoM shelves has been poorly quantified. This is specially truth for the southern part of GoM. Coupled models demonstrated to be an efficient tool to establish the routes of the TN (Fennel et al., 2006). In this sense Xue et al. (2013) proposed a first model for the TN dynamics for the GoM shelves, excluding however the YS. From our knowledge, there are no studies describing the nutrient flux pathways in the widest Yucatan shelf. Therefore, the present work represents the first quantitative analysis aiming to understand the biogeochemical cycles and their modulation by physical process at one of the most important socio-
15 economical areas of the southern Gulf of Mexico.

2 Model set-up and observational data

2.1 Physical model

The physical model is the Regional Ocean Modeling System (ROMS) which is a hydrostatic primitive equations model that uses orthogonal curvilinear coordinates in the horizontal and terrain following (*sigma*) coordinates in the vertical (Haidvogel and Beckmann, 1999). A full description of the model numerics can be found in Shchepetkin and McWilliams (2005) and Shchepetkin and McWilliams (2009). Horizontal grid resolution is ~ 5 km, with 36 modified *sigma* layers in the vertical. We used a new vertical stretching option (Azevedo Correia de Souza et al., 2015) that allows higher resolution near the surface. The numerical domain, which covers the whole GoM, is shown in the bathymetry map in Figure 1a. The model was ran for 20 years (1993 to 2012), from which we used 9 years (2002 to 2010) in the present analysis in order to be consistent with the
25 observational data.

The bathymetry is provided by a combination of the "General Bathymetric Chart of the Oceans" (GEBCO) database (<http://www.gebco.net/>) with data collected during several cruises in the GoM. The initial and boundary conditions for temperature, salinity and velocity come from the GLORYS2V3 reanalysis (Ferry et al., 2012). Hourly atmospheric forcing comes from the "Climate Forecast System Reanalysis" (CFSR) (Dee et al., 2014). These include cloud cover, 10 m winds, sea level atmospheric pressure, incident short and longwave radiation, latent and sensible heat fluxes, and air temperature and humidity
30 at 2 m. These variables are provided at ≈ 38 km horizontal resolution.



2.2 Biogeochemical model

The biogeochemical model is described in Fennel et al. (2006), and is based on the Fasham et al. (1990) model which takes Nitrogen based nutrients as limiting factor. The model is solved for seven state variables, namely: Nitrate (NO_3), Ammonium (NH_4), Phytoplankton (*Phy*), Zooplankton (*Zoo*), Chlorophyll (*Chl*), and two pools of detritus, Large Detritus (*LDet*) and Small Detritus (*SDet*). Details of the model algorithm and coupling to ROMS can be found in Fennel et al. (2006).

Initial and boundary conditions for the biogeochemical variables were obtained from an annual climatology of NO_3 , NH_4 and *Chl*. The climatology was calculated using all available profiles with the highest quality control from the World Ocean Database (Boyer et al., 2013), and profiles obtained from the XIXIMI cruises executed by the CICESE group. The DIVA optimal interpolation (Troupin et al., 2012) scheme was used to combine the individual profiles in the climatology using the model grid. DIVA takes into account the coast line geometry, sub-basins and advection to reduce errors due to artifacts in the interpolation.

However, it is well known that the available data density in the GoM is skewed towards the north. The XIXIMI cruises reduce this bias providing profiles of nutrients and chlorophyll in the southern GoM. The cruises encompass the region between 12°N and 26°N and -85°W and -97°W , and were executed within the scope of the “Consortio de Investigación del Golfo de México” (CIGoM) project (Gulf of Mexico Research Consortium project in English).

Close inspection of the shelf dynamics through maps of the temporally averaged velocity field $U=(\bar{u},\bar{v})$ (Figure 1b), where the overline denotes the temporal mean, and Mean Kinetic Energy $MKE=0.5(\bar{u}^2 + \bar{v}^2)$ (Figure 1c) allow to delimit the shelf into two areas. The first is the inner shelf, delimited by the 50 m isobath where the strongest velocities develop (Figure 1b) and where most of the MKE is enclosed (Figure 1c). The second area is the outer shelf between the 50 m and the 250 m isobaths, with the latter isobath representing the shelf break.

The TN examined in this study is taken as the sum of the Dissolved Inorganic Nitrogen (DIN) and the Particulate Organic Nitrogen (PON), with $\text{DIN} = \text{NO}_3 + \text{NH}_4$, and $\text{PON} = \text{Phy} + \text{Zoo} + \text{SDet} + \text{LDet}$. The cross-shelf nitrogen fluxes are calculated as:

$$Q_{50m,250m} = \int_{-50,-250}^{\eta} \mathbf{u}_{cross} N_z dz \quad (1)$$

where \mathbf{u}_{cross} is the velocity component normal to the 50 m or 250 m isobaths, η is the model sea level anomaly and N_z can be any component of the TN. Accordingly, the total budget is obtained as:

$$\int_{\sigma_n}^{\eta} \int_{y_n}^{y_1} \int_{x_n}^{x_1} (N_z) dx dy d\sigma = Q_{50m,250m} \quad (2)$$

where x , y and σ indicate longitude, latitude and sigma (terrain-following) layer, with n the number of horizontal grid points or vertical model layers.



The initial concentration of the biogeochemical variables (NH_4 , *Phy*, *Zoo*, *Chl*, and pools of detritus) is set to a small and positive value following Fennel et al. (2006, 2011); Xue et al. (2013). The biological model parameters used in this study are those shown in Table 1 of Fennel et al. (2006), except for the vertical sinking rates which were reduced about 10%, to fit the depth of the Deep Chlorophyll Maximum (DCM) observed with the APEX profiling floats (see Figure 3).

5 2.3 Freshwater sources

Two riverine systems account for 80% of the freshwater discharge into the GoM, the Mississippi/Atchafalaya system with $18,000 \text{ m}^3\text{s}^{-1}$, and Usumacinta/Grijalva system with $4500 \text{ m}^3\text{s}^{-1}$ (Dunn, 1996; Yáñez Arancibia and Day, 2004; Kemp et al., 2016). Riverine contributions to water volume, salinity, temperature and DIN concentration are included as grid-cell sources into the model. Apart from the two main systems, a total of 81 freshwater sources are included, taking account for freshwater discharges in the Florida, Texas and Yucatan shelves from years 1978 to 2015. For the US rivers the daily data were obtained from the U.S. Geological Survey (USGS) (<https://www.usgs.gov/>) and the Gulf of Mexico Coastal Ocean Observing System (GCOOS) (<https://products.gcoos.org/>). Monthly climatological values were calculated for the Mexican rivers, using temporally scattered information found in the literature (Rojas-Galaviz et al., 1992; Milliman and Syvitski, 1992; Poot-Delgado et al., 2015; Conan et al., 2016) and a data collection effort within Mexican institutions by Dr. Jorge Zavala-Hidalgo (*personal communication*). Therefore the US rivers present inter-annual variability but it is absent in the Mexican rivers.

Although the YS has no rivers, freshwater inputs play a key role impacting the local ecosystem (Herrera-Silveira et al., 2002). These inputs come from underwater groundwater sources linked to the “cenotes” (caves) system. The freshwater flux, temperature, salinity, and nutrient concentrations for these sources are not usually known. For modeling purposes, these are inversely estimated by adjusting the model results to the few temperature and salinity *in situ* data available and to chlorophyll satellite images.

The nitrogen concentration for freshwater sources is essentially DIN. For most of the northern rivers (e.g., Mississippi and Atchafalaya), PON is also considered (Fennel et al., 2011; Xue et al., 2013). For the remaining freshwater sources the PON contribution is set as a constant small value of 0.1 mmolN m^{-3} .

We also use hydrographic and biogeochemical observational stations taken during the GOMEX IV cruise in the study area. During this cruise a total of 71 profiles of NO_3 , potential temperature, salinity and chlorophyll were collected at standard depths in November 2015. The localization of the profiles are shown in Figure 2.

3 Model results evaluation

3.1 Basin model evaluation for the GoM

The lack of spatio-temporal biological data sets to validate biogeochemical models in the GoM is a well known problem (Walsh et al., 1989; Damien et al., 2018). The most abundant dataset is the satellite derived surface chlorophyll concentration. These observations give us a general overview of the chlorophyll temporal and spatial distribution patterns at basin scales.



Monthly mean time series (1998-2010) of chlorophyll-a concentration from Aqua-MODIS and SeaWiFS 9 km and 4 km (when available) satellite products are used for model evaluation. The temporal series averaged for the whole deep GoM (i.e., excluding high productive coastal areas with less than -1000 m depth) show a good agreement between the coupled model and the observations. The model tends to overestimate the *Chl* in winter and underestimation in summer (Figure 4). Despite some exceptional years (e.g., 1999), the modeled chlorophyll concentration values fall in the range exhibited by the satellite products. Mean satellital *Chl* is 0.1448 ± 0.04 mgChl m^{-3} in contrast with mean modelling *Chl* of 0.1433 ± 0.09 mgChl m^{-3} .

Observations of the chlorophyll vertical structure are available from eight APEX profiling floats with 537 profiles of *Chl* from 0 to 2000 m every ten days within the GoM (BOEM project) (Figure 3). A more detailed description of this database is provided by Hamilton et al. (2017), and the *Chl* data calibration by Pasqueron de Fommervault et al. (2017). The resulting profiles give valuable information to evaluate biogeochemical models through the water column, in contrast to the surface only information from satellite measurements (Pasqueron de Fommervault et al., 2017; Damien et al., 2018). The comparison shows that the model is able to reproduce the depth of the DCM measured by the floats. The DCM seasonal cycle is also well represented by the model. It is interesting to note the high dispersion in the data, revealing the large *Chl* variability found in the deep GoM.

The basin-scale physical validation of the model is presented in appendix A. The main features of the GoM variability are well represented by the model, specially the Loop Current which is a dominant player in the dynamics of the GoM. Climatology maps of sea surface temperature (SST) are also shown. The model is able to reproduce the seasonal cycles of both SST and mixed layer depth.

3.2 Regional model evaluation for the YS

The upwelling is more intense during Spring and weaker in Autumn as indicated in recent observational studies (Ruiz-Castillo et al., 2016). While the model presents upwelling during all the simulated months, this seasonal behavior is well represented in the climatologies obtained from the simulation results shown in Figure 2. The same figure also shows the position of the oceanographic stations occupied during the GOMEX IV cruise, and the delimitation of three areas of particular interest: the inner shelf, the outer shelf, and the upwelling region at Cape Catoche.

A point-by-point comparison between the model results and the *in situ* observations is shown using only data for November months from 2002 to 2010 in the model, for compatibility with the observation dates (Figures 5, 6 and 7). The range of temperatures at different depths shown by the model agrees well with those observed during the GOMEX IV (Figure 5). The mean observed temperature value is 25.5 ± 2.9 °C, while the model exhibits a mean temperature of 24.3 ± 3.7 °C. These differences [0.3 - 1.5] °C are considered acceptable considering there is no data assimilation in the model.

The simulated nutrient concentration depicts similar order of magnitude values (3.1 ± 4.8 mmolN m^{-3}) as the observed profiles (3.7 ± 5.2 mmolN m^{-3}) (Figure 6). Surface nutrient concentrations are underestimated by a 1.7 (mmolN m^{-3}) compared to observed profiles (Figure 6a). At subsurface depths (25 - 55 m), the model tends to underestimate the NO₃ concentrations, however, in the upwelling area, model NO₃ concentrations are closer to the observed values (Figure 6b). The temporal variabil-



ity of the modeled NO_3 is larger than the observed NO_3 at the surface and bottom as shown by the largest standard deviation in Figure 6b.

Below 55 m, both modeled and observed NO_3 are in good agreement in both, the outer shelf and the upwelling area (Figure 6c). Again, these model results are deemed consistent with observations (since there is no data assimilation) and in the range of other values reported in the literature (Merino, 1997). Since our knowledge, this is the first modeled study focus on the nitrate budget of the YS. Thereby, a direct comparison of the nitrate concentrations with other modeled results near the study area, e.g., Fennel et al. (2006) and Xue et al. (2013), is not straightforward because of the differences in the dynamics and the nitrate sources between the different shelves of the GoM.

For *Chl*, the model results fall within the range obtained from the fluorometer observations for the inner-, outer-shelf and upwelling area (Figure 7). The mean observed *Chl* ($0.52 \pm 0.6 \text{ mgChl m}^{-3}$) is slightly larger than the model results ($0.44 \pm 0.6 \text{ mgChl m}^{-3}$) but within the one standard deviation range, with mean differences between $[0.1 - 0.4] \text{ mgChl m}^{-3}$. Notice that there is agreement in *Chl* concentration between model and observations in the three layers between 150 m depth and the surface (Figures 7a, b and c).

4 Total Nitrogen budget and cross-shelf transports in the YS

The spatial averages of TN suggest a positive trend over the nine simulated years. This is observed for both the inner and the outer shelf (Figures 8a-d). The positive trend along time is also observed for temporal series of satellite chlorophyll, spatially averaged for the Yucatan Peninsula (Figure 8e), indicating that the modelled trend is not an artifact of the coupled model. In the inner shelf there are similar total integrated values of DIN and PON (Figure 8b), whereas in the outer shelf DIN values are larger than PON (Figure 8d). This is related to a very efficient biological cycle in terms of TN in the inner shelf, and to the fact that the integration in the outer shelf includes a large volume below the euphotic zone. The temporal series of the integrated TN show a combination of low frequency variability associated with the seasonal cycle and a high-frequency signal (periods lower than 30 days).

To understand the high variability in the YS-TN temporal series and to elucidate the contributions from different sources, the quantification of the cross-shelf fluxes becomes necessary. Their impact on the TN budget and the physical mechanisms modulating such fluxes are investigated next.

The cross-shelf fluxes are quantified for the two compartments, the inner and outer shelves (Figure 1b), and for all of the boundaries of each compartment. An schematic view of the main incoming and outgoing pathways of cross-shelf TN fluxes is shown in Figure 9. The yearly averages of the spatially integrated cross-shelf fluxes are shown in Table 1.

For the inner shelf, both PON and DIN are imported through its northern and eastern boundaries and exported through the west and south borders. The inner shelf acts as a source of PON for the Campeche basin at the southwest margin. The major source of TN for the inner is from the outer shelf through the Cape Catoche upwelling region, representing 80%. Freshwater sources contribute a 20%. Although this is a relatively high source of nitrogen, its relevance seems to be confined to the NW part of the inner-shelf. In general, there is a compensation between the DIN and PON concentrations in the inner-shelf (Figure



8b). This is attributed to an efficient biogeochemical cycle, where almost all the DIN imported into the shelf is consumed by the phytoplankton and thus converted into PON. This efficiency relies in the shallow water column of the inner shelf (50 m depth), meaning that the inner shelf is completely in the photic zone and under a strong mixing regime that redistributes the organic matter through the water column.

5 By contrast, in the outer shelf the largest inputs of PON and DIN are advected through its southeastern corner. The eastern boundary is a source of DIN but a sink of PON for the outer shelf. Therefore, the budget reveals that the PON exported to the inner shelf is produced in the outer shelf and not advected from Caribbean waters. The remaining TN flows escapes from the YS towards the deep GoM and the Campeche bay across the northern and western boundaries respectively. The contribution of TN from the inner shelf to the outer shelf represents only 1.5% of the total inputs.

10 Over the outer shelf the fluxes of nutrients and organic matter are driven by a westward wind driven circulation (Ruiz-Castillo et al., 2016) to be exported to the deep GoM through the north and to the Campeche basin through the west border. This represents a source of DIN, *Phy* and *Zoo* to the Campeche and the deep GoM, which are by definition oligotrophic areas.

In that regard, the model reveals a quasi-permanent thin filament of *Chl* that is advected from the northwest corner of the outer shelf to the west of the Campeche bay (Figure 10a). A vertical section along the 250 m isobath in the western YS (TN, Figure 10b) shows that while the export of organic matter to the open sea is concentrated in the surface layers (Figure 10d), the bottom layer presents a net DIN export (Figure 10c). The climatological average over nine years of simulated *Chl* show that this filament is intensified during winter times (not shown), although it is present during the whole simulated period. Sanvicente-Añorve et al. (2014) studied the larval dispersal for coral reef ecosystems in the southern GoM. They show that the northwestern corner of the outer YS acts as a sink region for larvae. Similar to other coral reef systems, they attributed the sink to the influence of the circulation patterns that lead to a unidirectional dispersion pattern during the whole year. Our model results support this idea providing nutrient dispersion patterns in the region over longer time periods.

Denitrification is a form of anaerobic microbial respiration in which nitrate and nitrite are finally reduced to dinitrogen. It represents a major sink for bioavailable nitrogen. Our results suggest that denitrification removes up to the 53% of the TN into the inner shelf, a significant percentage that agrees with estimates for other shelves in the GoM (Fennel et al., 2006). On the other hand, denitrification in the outer shelf only removes 9% of the TN. Our results also indicate that the denitrification rate tends to increase with time for both inner and outer shelves, similar to TN concentration (Figures 8a and c). This is expected since denitrification is a reduction process, hence an increase in the nitrate concentration means more available DIN to be reduced to dinitrogen.

4.1 Physical modulation of cross-shelf TN flux by CTWs

30 Many physical processes coexist at different spatio-temporal scales in the YS that modulate the cross-shelf transport of nutrients and organic matter. We suggest that at least two processes are responsible for such modulation: the CTWs and the interaction of the Yucatan Current with the shelf break.

CTWs can be generated by wind forcing over irregular bottom topography along the coast. These perturbations propagate with the shelf on their right in the northern hemisphere, and have been the subject of research for a long time (e.g., Clarke,



1977). The CTWs have a signature in the sea level, that is well captured in relatively high resolution models such as the one used in the present study (~ 5 km). These waves have been reported as being responsible for the modulation of upwelling systems such as the Australian coastal upwelling (Shaeffer et al., 2014). Few modelling and observational studies (Kolodziejczyk et al., 2011; Dubranna et al., 2011; Jouanno et al., 2016) describe the characteristics of CTWs in the GoM. In this study, the presence of CTWs is corroborated and its effect modulating the cross-shelf nutrient fluxes at the west margin of the YS is exposed.

The CTWs are remotely forced by alongshore winds, and occasionally in the Florida shelf (Dubranna et al., 2011; Jouanno et al., 2016), although are not necessarily ubiquitous of the northern part of the GoM. These waves then travel anti-clockwise with the coast on its right until they reach the western portion of the Yucatan peninsula. Observational and modelling studies pointed out that these waves cannot propagate beyond the Campeche shelf (Kolodziejczyk et al., 2011). The mechanism behind the vanishing of CTWs at the Campeche shelf may be related to a competition between the planetary β effect and the topography effect (Venegas-Vega, 2017). At the southern GoM the planetary effect induces the wave propagation and eddies to the west, while the topographic local effect induces a wave propagation towards the east. As a result, the propagation is inhibited at these places. The same pattern is present in the model simulations, as evidenced by the hovmoller diagram along the 50 m isobath shown in Figure 11. In agreement with previous observational and modelling studies of CTWs in the GoM (Dubranna et al., 2011; Jouanno et al., 2016), we find phase speeds in the range of $[2 - 4] \text{ m s}^{-1}$ (Figure 11b).

The multi-taper spectral analysis of Figure 12 (left hand figures) shows that the spectral shape and the range between 10 and 13 days of significant period peaks, are in close agreement between SLA and cross-shelf velocity time series (Figures 12a and b). Although similar peak periods between 7 and 12 days are found for the wind-stress time series (Figure 12c), the resemblance with the cross-shelf velocity is not so evident as for the SLA. Moreover, analysis of the wavelet power spectra of the cross-shelf velocity (Figure 12, right hand figures), sea level anomaly (Figure 12b) and the wind-stress (Figure 12c), shows that characteristic periods of the cross-shelf velocity in the 50 m isobath are well correlated with characteristic mean periods shown by the sea level anomaly temporal series ($r^2=0.41$). By contrast, these periods are not correlated with the mean periods exhibited by the local wind-stress ($r^2=0.16$). This shows that the ocean perturbations are remotely generated, with small influence from the local wind variability. The characteristic periods of each wavelet power spectrum are shown in Figure 12d. These periods are computed from the spectral wavelet analysis, by connecting periods of maximum power energy per day. The correlation coefficients found are statistically significant with p-values that greatly exceed the 95% confidence level. The mean and standard deviation of each time-series shown in Figure 12d are displayed in the wavelet power spectra. Notice that a mean period of 10.4 days for the cross-shelf velocity wavelet spectrum matches the mean period found for the SLAs.

The wavelet power spectrum analysis also provides a new view of the inter-annual variability of the nutrient flux. There are specific years in which the power increases. See for instance the years 2003, 2004, 2009 and 2010 in Figure 12a and b. These time intervals are consistent with years in which a El Niño Modoki or pseudo El Niño events are reported (Ashok et al., 2007; Ashok and Yamagata, 2009). For instance, Conan et al. (2016) suggest that El Niño Modoki 2009-2010 event influenced the biogeochemical cycling of phyto and bacterio-plankton communities in Términos Lagoon (South of GoM, in the Campeche shelf). They found that in this period the export of organic matter to the GoM was weak, making the Lagoon function as an nitrogen sink. This particular type of El Niño, is produced when the sea surface temperature warms in the central Pacific



(rather than in the western Pacific as the classic El Niño) and is surrounded by colder waters to the east and west. As a result wet conditions are produced in the central Pacific. There are evidences suggesting that El Niño Modoki can lead to an increase in the activity of tropical cyclones (Larson et al., 2012). Notice however that the year 2005, widely recognized to be the most intense hurricane season of the GoM, is not marked in the El Niño Modoki index and in the wavelet analysis presented here.

5 Hence, our analysis is not enough to draw any conclusion and further modeling and sampling effort research is needed.

4.2 Influence of the Yucatan Current in the coastal upwelling

Other physical mechanisms act to modulate the cross-shelf transport on the YS eastern and southeastern borders, specially affecting the DIN. The main import of TN to the YS is through the south, which can be related to advection by instabilities or encroachment of the intense Yucatan Current. This current flows from the Caribbean sea through the Yucatan channel to
10 finally become the Loop Current. Similarly, the export of TN to the deep GoM through the YS northern margin can be related to advection by the Yucatan Current and mesoscale structures.

However, this process can't be responsible for the second most important import of TN to the shelf at the eastern boundary. Here, other factors such as wind-induced upwelling at Cape Catoche and the interaction between the topography and the Yucatan Current can drive a TN flux to the YS (Jouanno et al., 2018). Previous observational studies found that the upwelling
15 at Cape Catoche is present all year (Ruiz-Castillo et al., 2016; Pérez-Santos et al., 2010), being more intense during spring time (Zavala-Hidalgo et al., 2006). The reason for this seasonality is not correlated with the Trade winds, since these are present throughout the year. Pérez-Santos et al. (2010), through ten years of sea surface wind data from the QuikSCAT satellite, found that the Ekman transport is the main contributor to the upwelling over the north YS (93 %), whereas the Ekman pumping only contributes the 7%. Therefore, the wind stress curl through classic Ekman pumping theory can not be the main driving
20 mechanism of the upwelling.

The interaction of the Yucatan current with the shelf break has been proposed as a mechanism to uplift deep waters into the shelf, feeding the upwelling process (Merino, 1997; Enriquez et al., 2013; Jouanno et al., 2018). Correlation analysis between the Yucatan Current and the TN, PON and DIN fluxes at the eastern margin show high values at interannual time scales (Figure 13). The trajectory of the Yucatan Current and its closeness to the YS has been also proposed as an upwelling mechanism
25 (Enriquez et al., 2010, 2013; Jouanno et al., 2018). When the Yucatan Current is closest to the Yucatan Peninsula, an increase in the sea surface height can be produced, favoring that Caribbean waters enters into the shelf. We have computed the closeness of the Yucatan Current core to the Cape Catoche and Notch areas, which are the two places where nutrients can be upwelled (not shown) (Jouanno et al., 2018). Our results pointed out that there is not a seasonality in the closeness of the current that explains the intensity of the upwelling during Spring or its weakness during Autumn. However, we found an smaller but
30 significant correlation with the sea surface height, supporting the reasoning of a dynamical upwelling due water accumulation in the coast. This analysis also show that the slope of the isotherm 22.5 °C, which traces the upwelled water (Cochrane, 1968; Merino, 1997), is slightly more steepness when the current core is close to the shelf.

This study suggests that, at the YS eastern boundary, the nutrient flux towards the coast can be driven by the Ekman bottom layer transport from the interaction of the Yucatan Current with the shelf break. The stress exerted by the intense along-shore



velocity of the Yucatan Current at the sharp shelf break produce a bottom Ekman spiral at the bottom. Similar to a surface Ekman spiral in the Northern Hemisphere, a northward along-shelf flow will generate a net depth integrated transport to the left in the bottom boundary layer, i.e., a cross-shelf transport towards the shelf. Similar mechanism has been for the southeastern Australian shelf Shaeffer et al. (2014). Using glider observations, the authors found that the bottom Ekman transport can explain up to the 71% of the bottom cross-shelf transport variability. It is worth noting that Sheinbaum et al. (2016), throughout three years of mooring measurements, show that the mean current near 1000 m oriented along the eastern edge of the YS flows towards the Caribbean sea, i.e., southwards. A southward flow at the eastern part of the YS will generate a coastal downwelling by an eastward Ekman transport. Notwithstanding, they also found that near surface, between 60 and 500 m, the mean current direction is northwest and its magnitude is stronger than the deepest southwards current.

Until now this process has not been fully tested. The present study provides a first modeling evidence that a bottom Ekman mechanism can be the precursor for the upwelling in Cape Catoche. The Bottom Ekman Transport (U_{bE} , $m^2 s^{-1}$) can be taken as $U_{bE} = -\tau_{by}/(\rho_o f)$, where τ_{by} is the bottom stress computed by $\tau_{by} = \rho_o C_d v_b \sqrt{u_b^2 + v_b^2}$, with $C_d = 1 \times 10^{-3}$ the drag coefficient, u_b and v_b are the bottom velocities at the 250 m isobath, f the Coriolis frequency and $\rho_o = 2015 \text{ kg m}^{-3}$ the reference potential density of the sea water. We found that U_{bE} is positive towards the shelf, and it is largely correlated with the bottom cross-shelf water transport ($r^2 = 0.71$, $ci = 95\%$) flowing towards the shelf (Figure 14a). The correlation is also large along time ($r^2 = 0.78$, $ci = 95\%$) as shown in Figure 14b. The comparison between the bottom layer Ekman transport and the time mean vertically integrated TN transport across the eastern 250 m isobath (Figure 14c) show that the Ekman transport is responsible for 65 % of the TN that is entering the shelf. The remaining flux in upper layers seems must be related to recirculation of the Yucatan Current by baroclinic meanders and small-scale structures whose role on the upwelling process needs to be further investigated.

Despite being an important mechanism acting to uplift nutrient-rich waters to the shelf helping the Cape Catoche upwelling, bottom Ekman transport is not the only possible mechanism. Other processes, such as the interaction of the Loop Current with the notch could develop intense vertical velocities thus enhancing the upwelling (Jouanno et al., 2018), encroachment of the current jet and mesoscale structures effects (Roughan and Middleton, 2002, 2004). Regarding current-topography interactions, Jouanno et al. (2018), by running a high-resolution model of the GoM, found that removing the notch from the bathymetry, the upwelling could be reduced in a 50% .

Here, we suggest that the upwelling of Cape Catoche is maintained by the combined effect of physical processes of topographic nature, in which the Ekman bottom transport has an important role, but is not the unique. Other processes, such as, current encroachment and eddy induced upwelling can have also important roles that must be analyzed in future research.

5 Concluding remarks

We present the results of a nine year simulation from a physical-biogeochemical coupled model for the GoM, focusing on the YS. The TN budget, main nutrient transport pathways and their modulation by physical process over the Yucatan shelf are



evaluated. Our work provides a first general view of the shelf physical-biogeochemical coupled system, schematized in Figure 15.

The results indicate that TN, especially DIN, enters the outer-shelf through the southern and eastern margins. The TN is then driven by a westward shelf current and is exported to the deep GoM and Campeche Sea through the northern and western boundaries, respectively. In the inner-shelf, the biogeochemical nitrogen-based cycle seems to be effective for NO_3 remineralization/consumption by the phytoplankton converting the DIN to PON. The freshwater sources represent an important contribution of about 20% to the DIN concentration, although it is restricted to the northwest of the Yucatan peninsula. The denitrification represents the main sink of nutrients for the inner shelf, removing more than the 50% of the nitrogen. Despite the inner shelf contributes to the TN to the west boundary of the outer shelf, this contribution is less than 2%, indicating low connectivity from the inner to the outer Yucatan shelf. On contrary, the outer shelf acts as the main nitrogen supply to the inner shelf, mainly of PON which comes from the eastern margin. Moreover, a quasi-constant filament in the west outer shelf border represent an important source of both organic and inorganic nitrogen for the oligotrophic Campeche sea.

While the surface Ekman layer at the western and northwestern outer shelf borders transport nutrient and organic matter to the Campeche Bay and the deep central GoM, this process is not able to explain the high-frequency variability of the TN cross-shelf fluxes. The results presented here show that such nitrogen fluxes are modulated by CTWs generated in the northern part of the GoM. These CTWs present mean periods of 10 days and phase speeds between 2 and 4 (m s^{-1}). The strength of this modulation can be reinforced depending on the wind conditions influenced by strong storms and hurricanes.

The advection by the Yucatan Current dominates the nutrient concentration import to the shelf through the southeast border. This advection, together with the influence of mesoscale structures control the export of nutrients to the deep GoM at the northern margin. A different process modulates the flux of nutrients at the eastern YS margin. Wind driven upwelling at Cape Catoche and the Yucatan Current flowing parallel to the slope play an important role in the intrusion of DIN into the shelf. Initial estimates carried out here suggest that the bottom Ekman layer transport explains the deep TN flux through the eastern YS boundary since there is a positive mean transport (into the shelf) over the nine simulated years along the the eastern shelf break. This indicates that the friction generated between the Yucatan Current and the shelf break can produce a bottom Ekman spiral with a net transport towards the shelf. Bottom Ekman transport can be arrested by stratification and may not be dominant everywhere along the YS east coast as has been documented in other western boundary upwelling regions (e.g., Roughan and Middleton, 2002, 2004).

Data availability. The data used in this study are available upon request to the corresponding author



Appendix A

A1 Basin scale model evaluation

This study is focused in the Yucatan shelf region whose hydrodynamics and biogeochemical outputs are previously validated. However, a general evaluation of the physical model ensures that the main dynamics of the whole GoM is correctly represented.

5 Thereby, the physical model is also evaluated in terms of their hydrography and general dynamics. Temporal averaged maps of eddy kinetic energy (EKE, $\text{m}^2 \text{s}^{-2}$) obtained from AVISO sea surface height are used to compare with the EKE computed by the model (Figures A1a and b) for 17 years (1995-2012). The model is able to capture the eddy field exhibited by the altimeter product. The main structure of the Loop Current is well represented by the model. In particular mean and variability of eddy kinetic energy field is reasonably captured by the model. A recognized feature is the hook-like pattern of EKE in the western part of the GoM, between 24 and 28 °N (Gough et al., 2019), and is more evident in the standard deviation of the EKE model (Figures A1c and d). This pattern is verified in both simulations and observations and is associated with a strong anticyclonic western boundary current that isolates the western continental shelf from the open ocean GoM. On the other hand, the enhancement of the EKE magnitude in ROMS, particularly at the Yucatan channel and Florida strait, is due to the higher resolution of the model (~ 5 km) respect to the altimeter product (~ 28 km).

15 Seasonal climatologies of the sea surface temperature (SST) are also compared with satellital product of Aqua-MODIS atmosphere products (<http://modis-atmos.gsfc.nasa.gov>) (Figure A2). The model SST shows a good agreement with both the interannual and seasonal cycles exhibited by the satellite. The overall bias for the deep GoM SST (depths > 1000 m) is in the range $[-0.21, +0.21]$ °C. Larger differences are found near coast. The model tends to underestimate the coastal SST during winter and spring times, while overestimates it during summer and autumn, respect to the satellital data. Nevertheless, these differences are less than 0.5 °C, and its average is in the order of 0.05 °C with an standard deviation of 0.4 °C. One of the reasons for this discrepancy lies in that satellite-derived provided the temperature relative only to a few microns of the sea surface, which is in fact named as the skin layer temperature (McKiver et al., 2016). Other reason can be also due to the representation of rivers, specially in the southern part of the GoM, where there exist a lack of temporal observations of the main freshwater sources. The river runoff can modify the surface thermal stratification inducing differences between the skin SST and the observed SST below 0.5 m approximately (Donlon et al., 2002).

25 In order to evaluate the mixed layer depth a total of 2629 ARGO floats profiles, availables in the time period between 1995-2012, are compared with the mixed layer depth given by the model in the deep GoM. This is an important quantity in terms of biogeochemical behavior, since the Gulf is an oligotrophic region in which primary production is controlled by the vertical advection of nutrients to the photic layer (Fennel et al., 2006; Xue et al., 2013; Damien et al., 2018). The biogeochemical cycles are partly controlled by the difference between the dark nutrient-rich waters and the upper ocean layer where the availability of light promotes the growth of phytoplankton and hence zooplankton. Figure A3 shows that the model is able to reproduce the seasonal cycle of the mixed layer in the GoM, with deepening during winter and shallowing during summer seasons (Damien et al., 2018; Portela et al., 2018). The model also shows shallower mixed layer depths during summer, and deepens during winter times respect to the Argo floats. The higher variability of the observed data are likely related with mesoscale structures



and submesoscale process which can locally deepening/shallowing the depth of the mixed layer (e.g., Boccaletti et al., 2007; Fox-Kemper et al., 2008; Levy et al., 2012). Moreover, physical processes developed below the 5 km of horizontal resolution are barely permitted by this model configuration. Despite the differences found, the bias between observations and model mixed layer depths are in the order of 1.4 m.

5 *Competing interests.* The authors declare that they have no conflict of interest

Acknowledgements. This research is funded by the National Council of Science and Technology of Mexico - Mexican Ministry of Energy-Hydrocarbon Trust, project 201441. This is a contribution of the Gulf of Mexico Research Consortium (CIGoM). The authors would like to thank the NASA Goddard Space Flight Center, Ocean Ecology Laboratory, Ocean Biology Processing Group. Moderate-resolution Imaging Spectroradiometer (MODIS) Aqua Chlorophyll Data; 2014 Reprocessing. NASA OB.DAAC, Greenbelt, MD, USA. doi: 10.5067/AQUA/MODIS/
10 L3M/CHL/2014 and to the Sea-viewing Wide Field-of-view Sensor (SeaWiFS) Chlorophyll Data; doi: 10.5067/ORBVIEW-2/SEAWIFS/
L3M/CHL/2014. The Ssalto/Duacs altimeter products were produced and distributed by the Copernicus Marine and Environment Monitoring Service (CMEMS) (<http://www.marine.copernicus.eu>). We acknowledge the provision of supercomputing facilities by CICESE. The authors are grateful to Dr Victor Camacho-Ibar (UABC) and Dr Sharon Herzka (CICESE), who provided nutrient data measured during the XIXIMI-IV cruise (funded by INECC-SEMARNAT, FOINS-CONACYT, Mexico). The APEX floats dataset were produced in the frame-
15 work of the “Lagrangian Study of the Deep Circulation in the Gulf of Mexico”, funded by the Bureau of Ocean and Energy Management, USA. Argo data were collected and made freely available by the International Argo Program and the national programs that contribute to it. (<http://www.argo.ucsd.edu>, <http://argo.jcommops.org>). The Argo Program is part of the Global Ocean Observing System. Argo float data and metadata from Global Data Assembly Centre (Argo GDAC). SEANOE. <http://doi.org/10.17882/42182>.



References

- Ashok, K. and Yamagata, T.: The El Niño with a difference, *Nature*, 461, 481–, <https://doi.org/10.1038/461481a>, 2009.
- Ashok, K., Behera, S. K., Rao, S. A., Weng, H., and Yamagata, T.: El Niño Modoki and its possible teleconnection, *Journal of Geophysical Research*, 112, <https://doi.org/10.1029/2006JC003798>, 2007.
- 5 Azevedo Correia de Souza, J., Powell, B., Castillo-Trujillo, A. C., and Flament, P.: The Vorticity Balance of the Ocean Surface in Hawaii from a Regional Reanalysis, *Journal of Physical Oceanography*, 45, 424–440, <https://doi.org/10.1175/JPO-D-14-0074.1>, <https://doi.org/10.1175/JPO-D-14-0074.1>, 2015.
- Boccaletti, G., Ferrari, R., and Fox-Kemper, B.: Mixed Layer Instabilities and Restratification, *Journal of Physical Oceanography*, 37, 2228–2250, <https://doi.org/10.1175/JPO3101.1>, <https://doi.org/10.1175/JPO3101.1>, 2007.
- 10 Boyer, T., Antonov, J. I., Baranova, O. K., Coleman, C., Garcia, H. E., Grodsky, A., Johnson, D. R., Locarnini, R. A., Mishonov, A. V., O'Brien, T., Paver, C., Reagan, J., Seidov, D., Smolyar, I. V., and Zweng, M. M.: World Ocean Database 2013, NOAA Atlas NESDIS 72, S. Levitus, Ed., A. Mishonov, Technical Ed.; Silver Spring, MD, 209 pp., <https://doi.org/10.7289/V5NZ85MT>, 2013.
- Bunge, L., Ochoa, J., Badan, A., Candela, J., and Sheinbaum, J.: Deep flows in the Yucatan Channel and their relation to changes in the Loop Current extension, *Journal of Geophysical Research*, 107, <https://doi.org/10.1029/2001JC001256>, 2002.
- 15 Clarke, A. J.: Observational and numerical evidence for wind-forced coastal trapped long waves, *Journal of Physical Oceanography*, 7, 231–247, [https://doi.org/10.1175/1520-0485\(1977\)007<0231:OANEFW>2.0.CO;2](https://doi.org/10.1175/1520-0485(1977)007<0231:OANEFW>2.0.CO;2), 1977.
- Cochrane, J.: Currents and Waters of the Eastern Gulf of Mexico and Western Caribbean, of the Western Tropical Atlantic Ocean, and of the Eastern Tropical Pacific Ocean, Houston, Texas: TAMU, Technical report No. 68-8T, pp. 19–28., 1968.
- Cochrane, J. D.: The Yucatan Current, upwelling off Northeastern Yucatan, and ccurrent and waters of Western Equatorial Atlantic., *Oceanography of the Gulf of Mexico. Progress Rep. TAMU Ref. No. 66-23T*, pp. 14-32, 1966.
- 20 Conan, P., Pujo-Pay, M., Agab, M., Calva-Benítez, L., Chifflet, S., Douillet, P., Dussud, C., Fichez, R., Grenz, C., Gutierrez-Mendieta, F., Origel-Moreno, M., Rodríguez-Blanco, R., Sauret, C., Severin, T., Tedetti, M., Torres-Alvarado, R., and J. F., G.: Biogeochemical cycling and phyto- and bacterio-plankton communities in a large and shallow tropical lagoon (Términos Lagoon, Mexico) under 2009-2010 El Niño Modoki drought conditions, *Biogeosciences*, 14, 959–975, <https://doi.org/10.5194/bg-14-959-2017>, 2016.
- 25 Damien, P., Pasqueron de Fommervault, O., Sheinbaum, J., Jouanno, J., and Duteil, O.: Partitioning of the Gulf of Mexico based on the seasonal and interannual variability of chlorophyll concentration, *Journal of Geophysical Research*, 2018.
- Dee, D. P., Balsameda, M., Balsamo, G., Engelen, R., Simmons, A. J., and Thépaut, J.-N.: Toward a Consistent Reanalysis of the Climate System, *Bulletin of the American Meteorological Society*, 95(8), 1235–1248, <https://doi.org/10.1175/BAMS-D-13-00043.1>, 2014.
- Donlon, C. J., Minnett, P. J., Gentemann, C., Nightingale, T. J., Barton, I. J., Ward, B., and Murray, M. J.: Toward improved validation of satellite sea surface skin temperature measurements for climate research, *J. Climate*, 15, 353–369, 2002.
- 30 Dubranna, J., Pérez-Brunius, P., López, M., and Candela, J.: Circulation over the continental shelf of the western and southwestern Gulf of Mexico, *Journal of Geophysical Research*, 116, <https://doi.org/10.1029/2011JC007007>, 2011.
- Dunn, D. D. .: Trends in Nutrient Inflows to the Gulf of Mexico from Streams Draining the Conterminous United States 1972 - 1993, U.S. Geological Survey, Water-Resources Investigations Report 96-4113. Austin, Texas: U.S. Geological Survey. 60 pp., 1996.
- 35 Enriquez, C., Mariño Tapia, I., and Herrera-Silveira, J.: Dispersion in the Yucatan coastal zone: Implications for red tide events, *Continental Shelf Research*, 30, 127–137, <https://doi.org/10.1016/j.csr.2009.10.005>, 2010.



- Enriquez, C., Mariño Tapia, I., Jeronimo, G., and Capurro-Filigrasso, L.: Thermohaline processes in a tropical coastal zone, *Continental Shelf Research*, 69, 101–109, <https://doi.org/10.1016/j.csr.2013.08.018>, 2013.
- Fasham, M. J. R., Ducklow, H. W., and McKelvie, S. M.: A nitrogen based model of plankton dynamics in the oceanic mixed layer, *Journal of Marine Research*, 48, 591 – 639, 1990.
- 5 Fennel, K.: The role of continental shelves in nitrogen and carbon cycling: Northwestern North Atlantic case study, *Ocean Sci.*, 6, 539–548, <https://doi.org/10.5194/os-6-539-2010>, 2010, 2010.
- Fennel, K., Wilkin, J., Levin, J., Moisan, J., O'Reilly, J., and Haidvogel, D.: Nitrogen cycling in the Middle Atlantic Bight: results from a three-dimensional model and implications for the North Atlantic nitrogen budget, *Global Biogeochemical Cycles*, 20, <https://doi.org/10.1029/2005GB002456>, 2006.
- 10 Fennel, K., Hetland, R., Feng, Y., and DiMarco, S.: A coupled physical-biological model of the Northern Gulf of Mexico shelf: Model description, validation and analysis of phytoplankton variability, *Biogeosciences*, 8, 1881–1899, 2011.
- Ferry, N., Parent, L., Garric, G., Drevillon, M., Desportes, C., Bricaud, C., and Hernandez, F.: Scientific Validation Report (ScVR) for reprocessed analysis and reanalysis, MyOcean Project Rep., WP04-GLO-MERCATOR, MYO-WP04-ScCV-rea-MERCATOR-V1.0, Toulouse, France., 2012.
- 15 Fox-Kemper, B., Ferrari, R., and Hallberg, R.: Parameterization of Mixed Layer Eddies. Part I: Theory and Diagnosis, *Journal of Physical Oceanography*, 38, 1145–1165, <https://doi.org/10.1175/2007JPO3792.1>, <https://doi.org/10.1175/2007JPO3792.1>, 2008.
- Gallardo, A. and Marui, A.: Submarine groundwater discharge: an outlook of recent advances and current knowledge, *Geo-Marine Letters*, 26, 102–113, 2006.
- Gough, M. K., Beron-Vera, F. J., Olascoaga, M. J., Sheinbaum, J., Jouanno, J., and Duran, R.: Persistent transport pathways in the northwest-
20 ern Gulf of Mexico, *J. Phys. Oceanogr.*, 49, 353–367, <https://doi.org/10.1175/JPO-D-17-0207.1>, 2019.
- Gutierrez-de Velasco, G. and Winant, D.: Seasonal patterns of wind stress and stress curl over the Gulf of Mexico, *J. Geophys. Res.*, 101, 18 127–18 140, 1996.
- Haidvogel, D. B. and Beckmann, A.: *Numerical Ocean Circulation Modeling*, Imperial College Press, 1999.
- Hamilton, P., Bower, A., Furey, H., Leben, R., and Pérez-Brunius, P.: *Deep Circulation in the Gulf of Mexico: A Lagrangian Study.*, U.S.
25 Dept. of the Interior, Bureau of Ocean Energy Management, Gulf of Mexico OCS Region, New Orleans, LA. OCS Study BOEM 2017-0xx. 285 pp., 2017.
- Hermann, A., Hinckley, S., Dobbins, E. L., Haidvogel, D. B., Bond, N. A., Mordy, C., Kachel, N., and Stabeno, P. J.: Quantifying cross-shelf and vertical nutrient flux in the Coastal Gulf of Alaska with a spatially nested, coupled biophysical model, *Deep Sea Research Part II: Topical Studies in Oceanography*, 56, 2474 – 2486, <https://doi.org/https://doi.org/10.1016/j.dsr2.2009.02.008>, <http://www.sciencedirect.com/science/article/pii/S0967064509000484>, 2009.
30
- Herrera-Silveira, J., Medina-Gomez, I., and Colli, R.: Trophic status based on nutrient concentration scales and primary producers community of tropical coastal lagoons influenced by groundwater discharges, *Hydrobiologia*, 475, 91–98, 2002.
- Herrera-Silveira, J., Comin, F., Aranda-Cicerol, N., Troccoli, L., and Capurro, L.: Coastal water quality assessment in the Yucatan peninsula: management Implications, *Ocean and Coastal Management*, 47, 625–639, 2004.
- 35 Jouanno, J., Ochoa, K., Pallàs-Sanz, E., Sheinbaum, J., Andrade, F., Candela, J., and Molines, J.: Loop Current Frontal Eddies: Formation along the Campeche Bank and Impact of Coastally Trapped Waves, *Journal of Physical Oceanography*, 46, 3339–3363, <https://doi.org/10.1175/JPO-D-16-0052.1>, 2016.



- Jouanno, J., Pallàs-Sanz, E., and Sheinbaum, J.: Variability and Dynamics of the Yucatan Upwelling: High-Resolution Simulations, *Journal of Geophysical Research: Oceans*, 123, <https://doi.org/10.1002/2017JC013535>, 2018.
- Kemp, G. P., Day, J. W., Yáñez-Arancibia, A., and Peyronnin, N. S.: Can Continental Shelf River Plumes in the Northern and Southern Gulf of Mexico Promote Ecological Resilience in a Time of Climate Change?, *Water*, 8, <https://doi.org/10.3390/w8030083>, <http://www.mdpi.com/2073-4441/8/3/83>, 2016.
- 5 Kolodziejczyk, N., Ochoa, J., Candela, J., and Sheinbaum, J.: Deep Currents in the Bay of Campeche, *Journal of Physical Oceanography*, 41, 1902–1920, <https://doi.org/10.1175/2011JPO4526.1>, 2011.
- Larson, S., Lee, S., Wang, C., Chung, E., and Enfield, D.: Impacts of noncanonical El Niño patterns on Atlantic hurricane activity, *Geophys. Res. Lett.*, 39, <https://doi.org/10.1029/2012GL052595>, 2012.
- 10 Levy, M., Iovino, D., Resplandy, L., Klein, P., Madec, G., Treguier, A.-M., Masson, S., and Takahashi, K.: Large-scale impacts of submesoscale dynamics on phytoplankton: Local and remote effects, *Ocean Modelling*, 43–44, 77 – 93, <https://doi.org/10.1016/j.ocemod.2011.12.003>, 2012.
- Liu, K.-K., Atkinson, L., Quinones, R., and Talaue-McManus, L.: *Carbon and Nutrient Fluxes in Continental Margins: A Global Synthesis*, IGBP Book Series, Berlin., 2010.
- 15 McKiver, W. J., Sannino, G., Braga, F., and Bellafore, D.: Investigation of model capability in capturing vertical hydrodynamic coastal processes: a case study in the north Adriatic Sea, *Ocean Sci.*, 12, 51–69, <https://doi.org/doi.org/10.5194/os-12-51-2016>, 2016.
- Merino, M.: Upwelling on the Yucatan shelf: hydrographic evidence, *Journal of marine systems*, 13, 101–121, 1997.
- Milliman, J. and Syvitski, J.: Geomorphic/tectonic control of sediment discharge to the ocean: the importance of small mountainous rivers, *Journal of Geology*, 100, 525–544, 1992.
- 20 Ochoa, P., Sheinbaum, J., Badan, A., Candela, J., and Wilson, D.: Geostrophy via potential vorticity inversion in the Yucatan Channel, *J. Mar. Res.*, 59, 725–747, 2001.
- Pasqueron de Fommervault, O., D’Ortenzio, F., Mangin, A., Serra, R., Migon, C., Claustre, H., and Schmechtig, C.: Seasonal variability of nutrient concentrations in the Mediterranean Sea: Contribution of Bio-Argo floats., *Journal of Geophysical Research: Oceans*, 2015.
- Pasqueron de Fommervault, O., Pérez-Brunius, P., Damien, P., and Sheinbaum-Pardo, J.: Temporal variability of chlorophyll distribution in
25 the Gulf of Mexico: bio-optical data from profiling floats, *Biogeosciences Discussions*, 2017.
- Pérez-Santos, I., Schneider, W., Sobarzo, M., Montoya-Sánchez, R., Valle-Levinson, A., and Garcés-Vargas, J.: Surface wind variability and its implications for the Yucatan basin Caribbean Sea dynamics, *Journal of Geophysical Research*, 115, <https://doi.org/10.1029/2010JC006292>, 2010.
- Poot-Delgado, C. A., Okolodkov, Y. B., Aké-Castillo, J. A., and von Osten, J. R.: Annual cycle of phytoplankton with emphasis on potentially
30 harmful species in oyster beds of Terminos Lagoon, southeastern Gulf of Mexico., *Revista de Biología Marina y Oceanografía*, 50, 465–477, <https://doi.org/10.4067/S0718-19572015000400006>, 2015.
- Pope, K. O., Ocampo, A. C., and Duller, C. E.: Mexican site for K/T impact crater, *Nature*, 351, 105, 1191.
- Portela, E., Tenreiro, M., Pallàs-Sanz, E., Meunier, T., Ruiz-Angulo, A., Sosa-Gutiérrez, R., and Cusí, S.: Hydrography of the central and western Gulf of Mexico. *Journal of Geophysical Research*, 123, 5134–5149,
35 <https://doi.org/10.1029/2018JC013813>, 2018.
- Reyes-Mendoza, O., Mariño Tapia, I., Herrera-Silveira, J., Ruiz-Martínez, G., Enriquez, C., and Largier, J. L.: The Effects of Wind on Upwelling off Cabo Catoche, *Journal of Coastal Research*, 32, 638 – 650, <https://doi.org/10.2112/JCOASTRES-D-15-00043.1>, 2016.



- Rojas-Galaviz, J., Yaáñez Arancibia, A., Day, J., and Vera-Herrera, F.: Estuarine Primary Producers: Laguna de Terminos—a Study Case, In, U. Seeliger, ed., *Coastal Plant Communities of Latin America*. San Diego: Academic Press., 1992.
- Roughan, M. and Middleton, J.: A comparison of observed upwelling mechanisms off the east coast of Australia, *Continental Shelf Research*, 22, 2551–2572, [https://doi.org/10.1016/S0278-4343\(02\)00101-2](https://doi.org/10.1016/S0278-4343(02)00101-2), 2002.
- 5 Roughan, M. and Middleton, J.: On the East Australian Current: Variability, encroachment, and upwelling, *Journal of Geophysical Research*, 109, <https://doi.org/10.1029/2003JC001833>, 2004.
- Ruiz-Castillo, E., Gomez-Valdes, J., Sheinbaum, J., and Rioja-Nieto, R.: Wind-driven coastal upwelling and westward circulation in the Yucatan shelf, *Continental Shelf Research*, 118, 63–76, <https://doi.org/10.1016/j.csr.2016.02.010>, 2016.
- Sanvicente-Añorve, L., Zavala-Hidalgo, J., Allende-Arandía, M. E., and Hermoso-Salazar, M.: Connectivity patterns among coral reef systems in the southern Gulf of Mexico, *Marine Ecology Progress Series*, 498, 27–41, <https://doi.org/10.3354/meps10631>, 2014.
- 10 Seitzinger, S., Harrison, J. A., Böhlke, J. K., Bouwman, A. F., Lowrance, R., Peterson, B., Tobias, C., and Dreht, G. V.: Denitrification across landscapes and waterscapes: a synthesis., *Ecological Applications*, 16, 2064–2090, [https://doi.org/10.1890/1051-0761\(2006\)016\[2064:DALAWA\]2.0.CO;2](https://doi.org/10.1890/1051-0761(2006)016[2064:DALAWA]2.0.CO;2), 2006.
- Shaeffer, A., Roughan, M., and Wood, J.: Observed bottom boundary layer transport and uplift on the continental shelf adjacent to a western boundary current, *J. Geophys. Res. Oceans*, 119, 4922–4939, <https://doi.org/10.1002/2013JC009735>, 2014.
- 15 Shchepetkin, A. F. and McWilliams, J. C.: The Regional Oceanic Modeling System (ROMS): a split-explicit, free-surface, topography-following-coordinate oceanic model, *Ocean. Model.*, 9, 347–404, 2005.
- Shchepetkin, A. F. and McWilliams, J. C.: Correction and commentary for “Ocean forecasting in terrain-following coordinates: Formulation and skill assessment of the regional ocean modeling system” by Haidvogel et al. *J. Comp. Phys.* 227, pp. 3595–3624, *J. Comput. Phys.*, 20, 228, 8985–9000, 2009.
- Sheinbaum, J., Candela, J., Badan, A., and Ochoa, J.: Flow structure and transport in the Yucatan Channel, *Geophys. Res. Lett.*, 29, 2002.
- Sheinbaum, J., Athié, G., Candela, J., Ochoa, J., and A., R.-A.: Structure and variability of the Yucatan and loop currents along the slope and shelf break of the Yucatan channel and Campeche bank, *Dynamics of Atmospheres and Oceans*, 76, 217–239, <https://doi.org/10.1016/j.dynatmoce.2016.08.001>, 2016.
- 25 Troupin, C., Barth, A., Sirjacobs, D., Ouberdous, M., Brankart, J.-M., Brasseur, P., Rixen, M., Alvera Azcarate, A., Belounis, M., Capet, A., Lenartz, F., Toussaint, M.-E., and Beckers, J.-M.: Generation of analysis and consistent error fields using the Data Interpolating Variational Analysis (Diva), *Ocean Modelling*, 52–53, 90–101, <https://doi.org/10.1016/j.ocemod.2012.05.002>, 2012.
- Venegas-Vega, F.: Wind-driven circulation in a closed basin with variable topography, Master’s thesis, Centro de Investigación Científica y de Educación Superior de Ensenada, Baja California, Mexico, 2017.
- 30 Walsh, J. J., Dieterle, D. A., Meyers, M. B., and Müller-Karger, F. E.: Nitrogen exchange at the continental margin: A numerical study of the Gulf of Mexico, *Prog. Oceanogr.*, 23, 245–301, 1989.
- Xue, Z., He, R., Fennel, K., Cai, W.-J., Lohrenz, S., and Hopkinson, C.: Modeling ocean circulation and biogeochemical variability in the Gulf of Mexico, *Biogeosciences*, 10, 7219–7234, <https://doi.org/10.5194/bg-10-7219-2013>, 2013.
- Yáñez Arancibia, A. and Day, J.: The Gulf of Mexico: Towards an integration of coastal management with large marine ecosystem management, *Ocean Coast. Manag.*, 47, 537–563, 2004.
- 35 Zavala-Hidalgo, J., Gallegos-García, A., Martínez-López, B., Morey, S., and O’Brien, J. J.: Seasonal upwelling on the western and southern shelves of the Gulf of Mexico, *Ocean Dynamics*, 56, 333–338, 2006.



Zavala-Hidalgo, J., R., R.-C., A., M.-J., Morey, S. L., and Martínez-López, B.: The response of the Gulf of Mexico to wind and heat flux forcing: What has been learned in recent years?, *Atmósfera*, 27, 317 – 334, [https://doi.org/10.1016/S0187-6236\(14\)71119-1](https://doi.org/10.1016/S0187-6236(14)71119-1), <http://www.sciencedirect.com/science/article/pii/S0187623614711191>, 2014.



Table 1. Nutrient budget in molN yr^{-1} for the inner (50 m isobath) and outer (250 m isobath) of the Yucatan shelf, computed at each boundary (N, W, E and S) by using projected cross-shelf velocities. The flux of nutrients is integrated through the water column and temporally averaged. Years from 2002 to 2010 are used to compute the budget. Positive values means source of nutrients, whereas negative values represent sinks of TN as denitrification is always a nitrogen removal process.

Boundary	PON	DIN	TN	Fresh water/Inner ^a
Inner-shelf budget ($\times 10^{10} \text{ molN yr}^{-1}$)				
N	0.34	1.63	1.97	0.76
W	-0.72	-0.02	-0.73	0.72
E	2.35	1.68	4.32	0
S	-2.29	-0.05	-2.34	0
Denitrification	-3.34			
Trend ^b	-0.64			
Outer-shelf budget ($\times 10^{10} \text{ molN yr}^{-1}$)				
N	-11.46	-7.42	-18.88	-1.97
W	-1.85	-9.87	-11.72	0.72
E	-0.28	7.65	7.36	-4.03
S	11.17	27.74	38.92	0
Denitrification	-3.34			
Trend ^b	-0.66			

^aFresh water sources are considered only for the inner-shelf. Inner can be taken as a source or sink of nitrogen only for the outer-shelf.

^bThe positive trend of total nitrogen observed in the temporal series during nine years is also taken into consideration to close the budget.

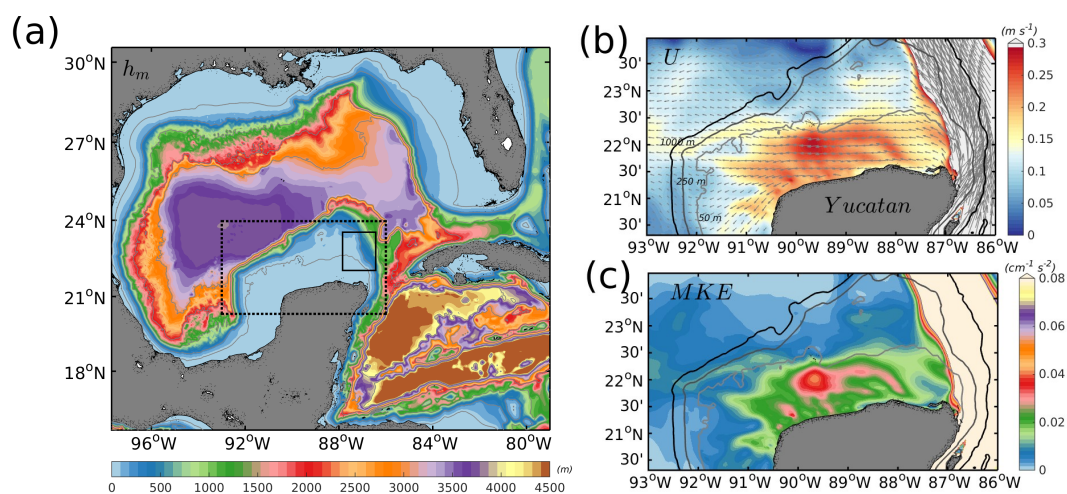


Figure 1. Bathymetry (h_m , m) of the whole model domain. Isobaths: 50, 250, 1000, 2000, 3000 and 4000 m are also shown in gray contours. The black dashed box delimits the study area of the Yucatan shelf, where (b) is the surface temporally averaged velocity field (U , m s^{-1}) with magnitude in color and vectors representing the direction; and (c) is the surface Mean Kinetic Energy (MKE, $\text{cm}^2 \text{s}^{-2}$) computed for the year 2010. The smallest black box in (a) shows the “notch” area.

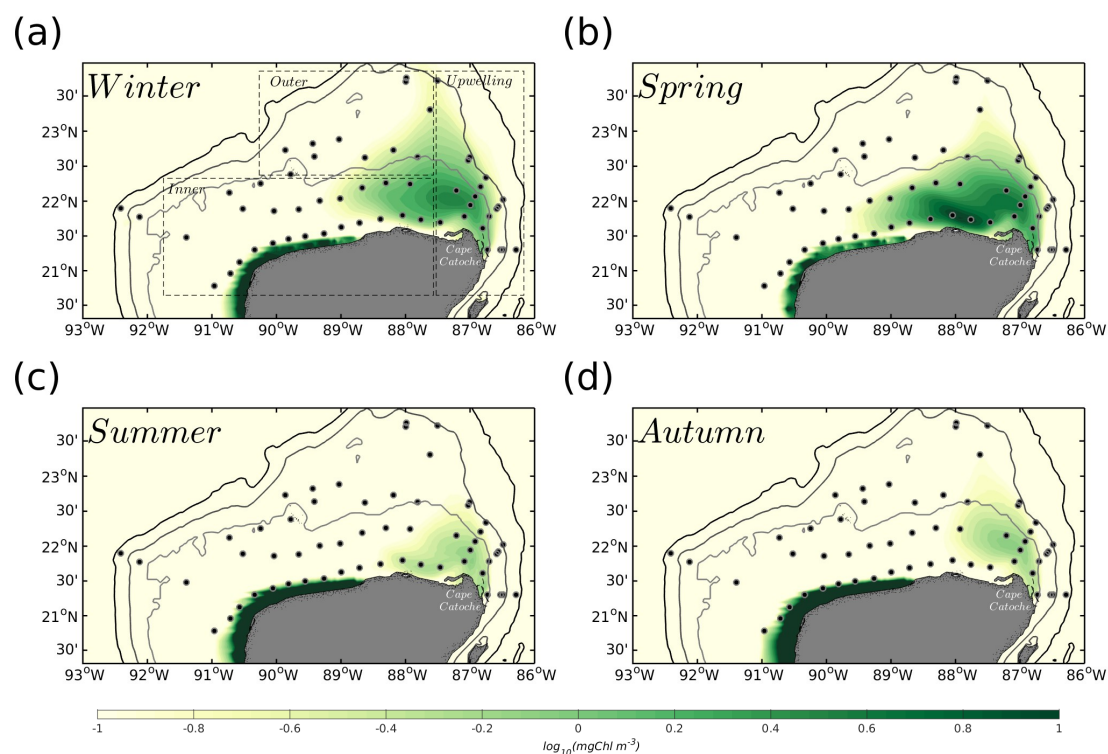


Figure 2. Seasonal climatology of surface chlorophyll given by the biogeochemical coupled model for: (a) Winter (Jan, Feb, Mar); (b) Spring (Apr, May, Jun); (c) Summer (Jul, Aug, Sep) and (d) Autumn (Oct, Nov, Dec), for the period between 2002 and 2010. Dashed boxes in (a) denote the three areas in which the validation with observations (black dots) was carried out, i.e., inner shelf, outer shelf and the upwelling region close to Cape Catoche.

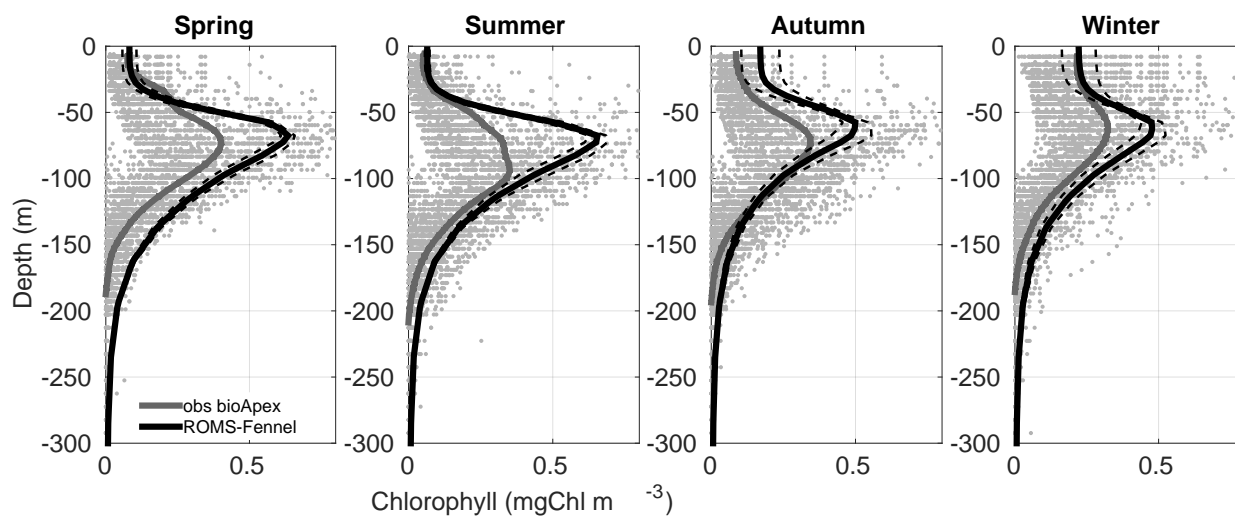


Figure 3. Seasonal comparison of chlorophyll profiles in mgChl m^{-3} , taking all the available Apex floats (Pasqueron de Fommervault et al., 2015), in order to evaluate the Deep Chlorophyll Maximum (DCM). Grey dots are the data observed from Apex floats, gray profile is the average profile. Black profile is the averaged profile of the model data with its respective standard deviation in dashed black lines.

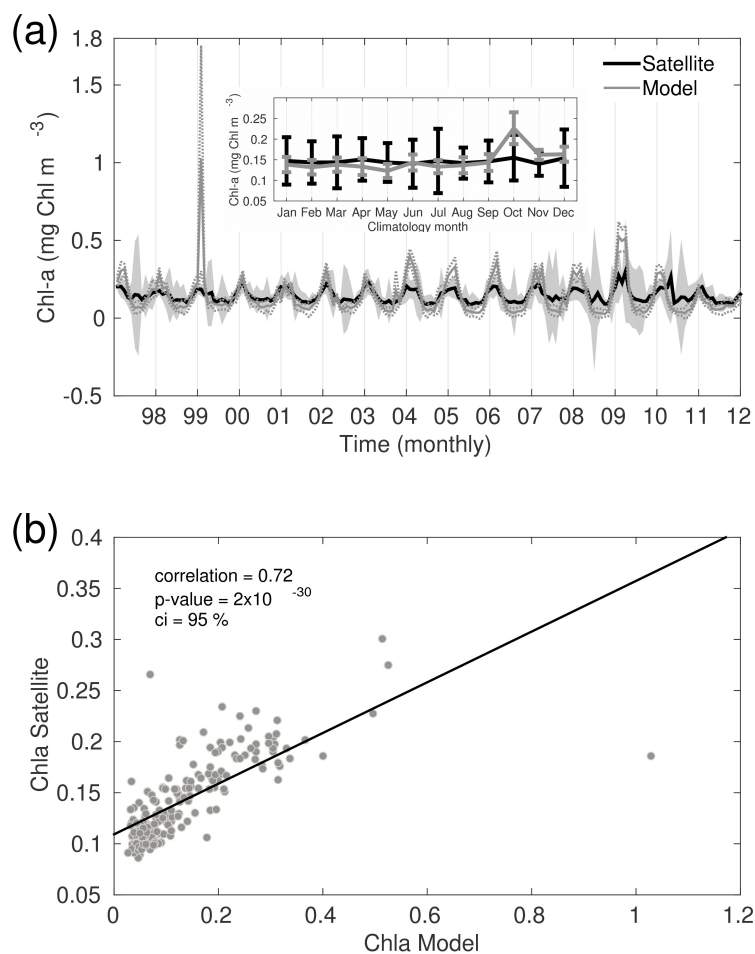


Figure 4. Comparison of surface chlorophyll in mgChl m^{-3} between satellite and model for the whole deep GoM in terms of temporal series (a). Standard deviation from the spatial averages are shown in shadow areas for satellite and in dashed lines for model. The monthly climatology of the temporal series is show at the upper part of the figure, where vertical bars indicate standard deviation from the temporal mean. In (b) are represented the correlation coefficient of both monthly temporal series and their respective linear fit in black line.

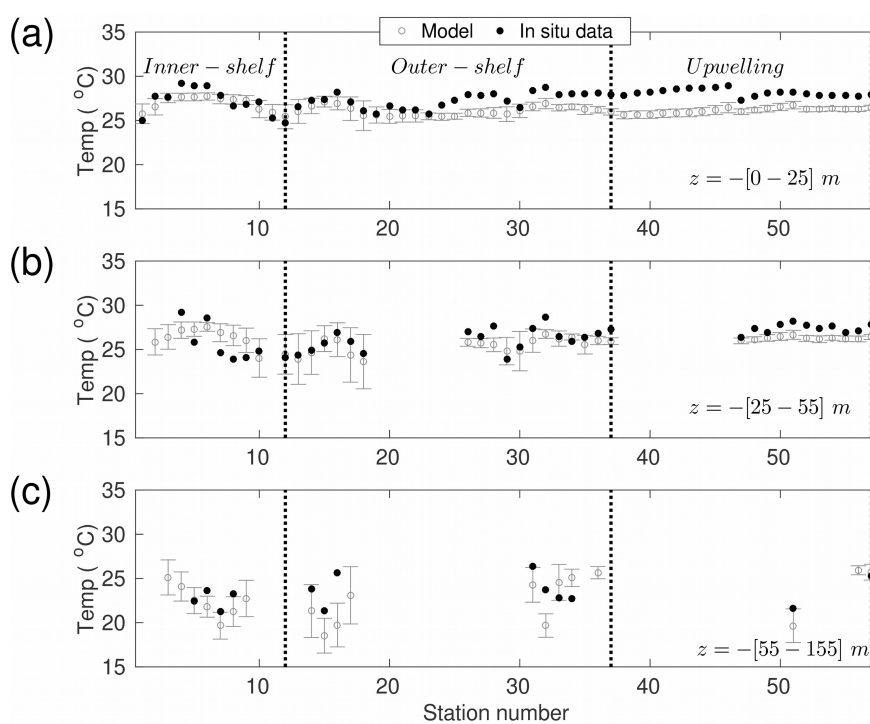


Figure 5. Comparison between in situ data and simulated temperatures (T °C). Temperatures values correspond to a each hydrographic station, averaged over three depths; (a) between surface and 25 m depth, (b) between 25 and 50 m depth, and (c) between 55 and the deepest measured concentration ($z \sim -150$ m). Black dots correspond to the observed values and open gray circles to the simulated variable. Vertical gray lines are the temporal standard deviation for the simulated values, as these are temporally averaged over all Novembers from 2002 to 2010. Vertical black lines delimit the group of stations for inner-shelf, outer-shelf and the upwelling area.

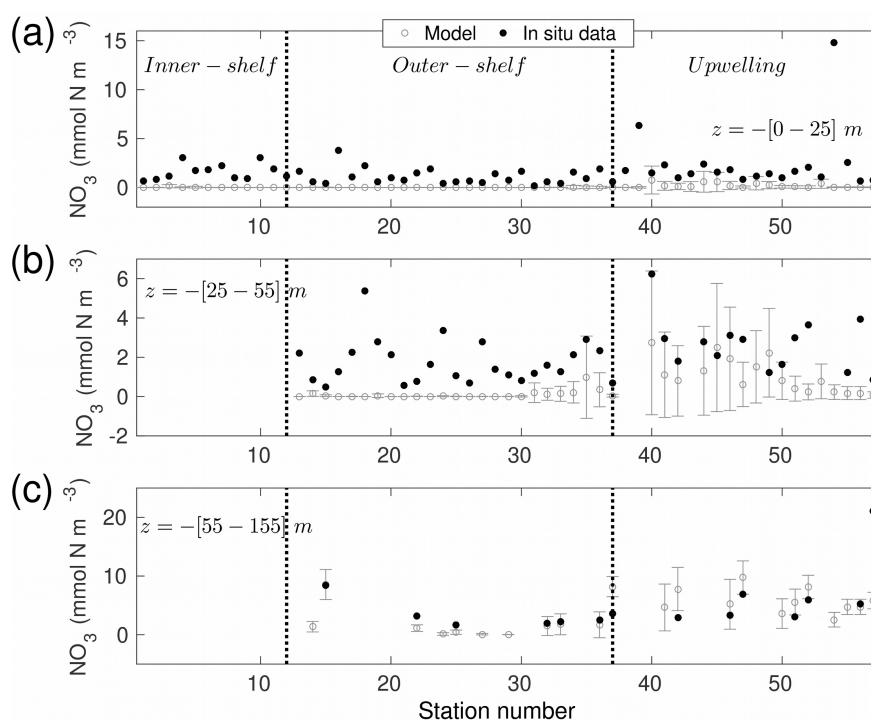


Figure 6. Same as Figure 5, but for nitrate concentrations in mmol N m^{-3} .

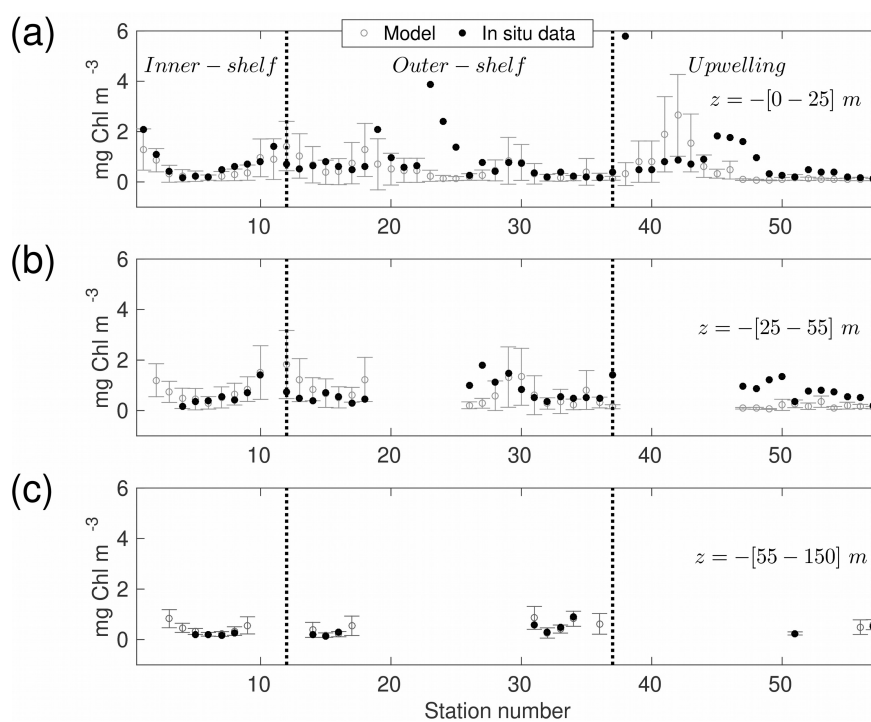


Figure 7. Same as Figure 5, but for chlorophyll concentrations in mg Chl m⁻³.

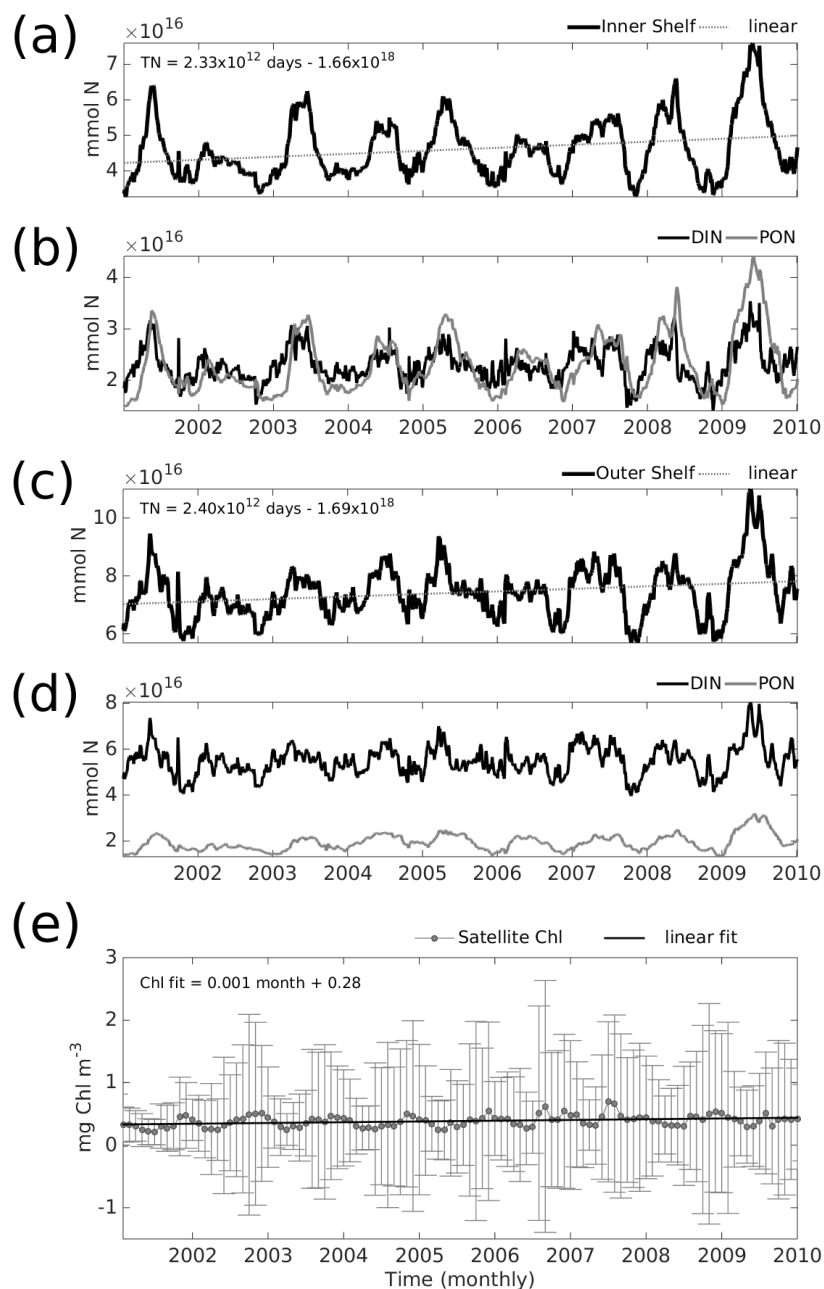


Figure 8. Temporal series of TN, PON and DIN, integrated over the area of the inner shelf (a) and (b), and over the area of the outer shelf (c) and (d). Temporal series of monthly satellite chlorophyll averaged over the YS area (e), where gray vertical bars indicate standard deviation. The equation of each linear fit is shown at the top of (a), (c) and (e)

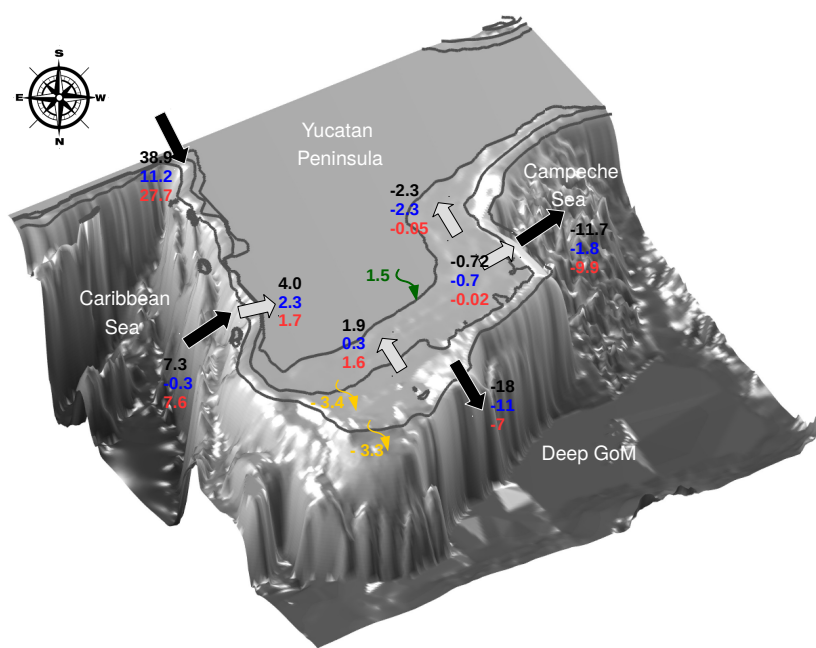


Figure 9. Scheme of the Total Nitrogen (TN) budget for the Yucatan shelf. Black arrows and contour denote cross-shelf direction flux and the 250 m isobath delimiting the outer shelf. Gray arrows and contour are analogous to the black but for the inner shelf delimited by the 50 m isobath. In blue are the Dissolved Inorganic Nitrogen (DIN); in red the Particulate Organic Nitrogen (PON); freshwater DIN sources (Rivers) are in green and sinks of TN due denitrification (DNF) are in yellow. The values are expressed in $\text{mmolN s}^{-1} \times 10^{13}$. Negative values indicate sink, whereas positive indicates source of TN.

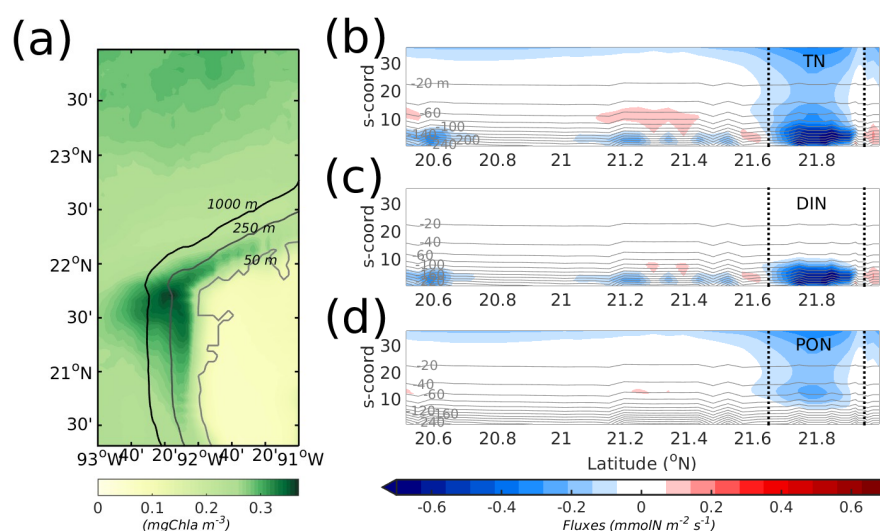


Figure 10. (a) Map of surface chlorophyll in mgChla m^{-3} , averaged over the nine simulated years. The three characteristic isobaths are denoted. Flux vertical sections along the 250 m isobath at the western boundary of (b) Total nitrogen, (c) DIN and (d) PON in ($\text{mmolN m}^{-2} \text{s}^{-1}$). Negative values indicate westward flux, i.e., TN flux from the shelf to the Campeche sea. The area delimited by dashed lines show the location of the filament depicted in (a), at the NW of the YS. Notice that vertical sections are plotted against the model vertical coordinate system. The depths in m are indicated as horizontal gray lines.

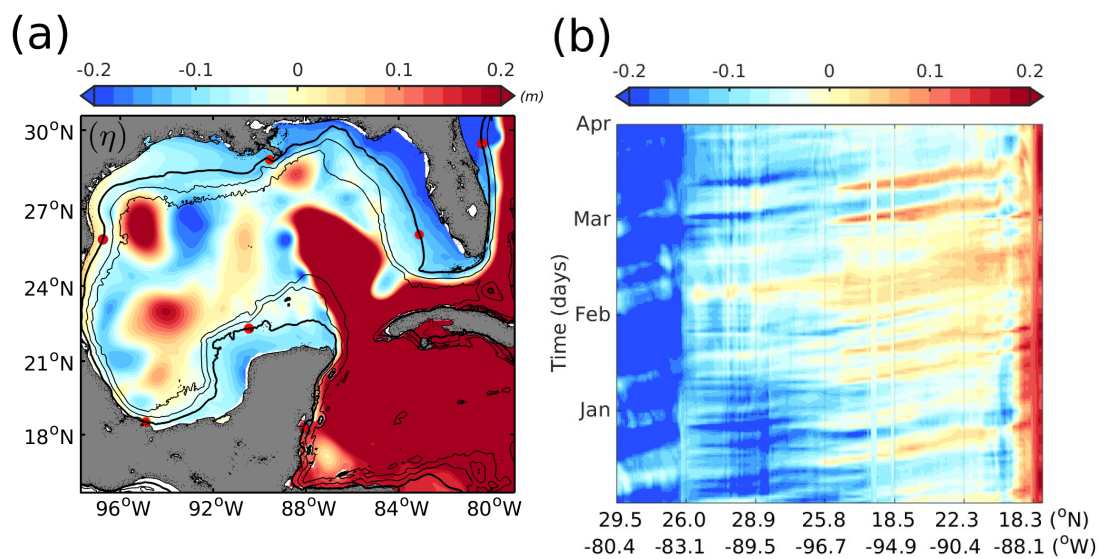


Figure 11. (a) Snapshot of sea level anomaly (η , m) for the simulated year 2005. (b) Hovmoller diagram of η along the 50 m isobath from January to April of the 2005 year. Red dots in (a) denote the latitude and longitude shown at the bottom of (b), from Florida to Yucatan peninsula.

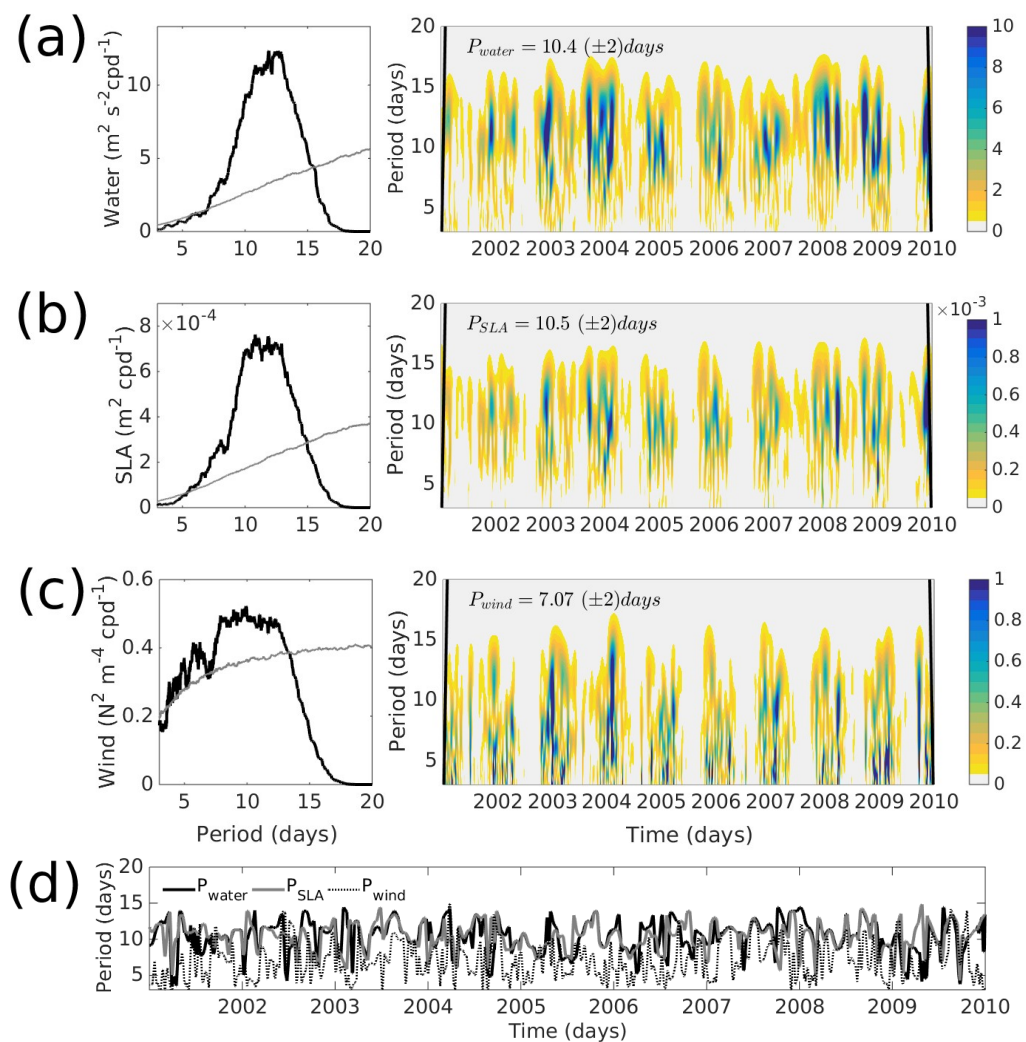


Figure 12. Multi-taper spectrum (black line) on the left hand side figures for time-series of west 50 m isobath of (a) cross-shelf velocity current; (b) sea level anomaly (SLA), and (c) wind-stress. The temporal series are previously detrended and filtered with a lanczos high-pass filter with a cut-off of 15 days in order to remove low frequency process. The multi-taper spectra are built with 30 tapers or windows. The significance levels relative to the estimated noise background of 99% is shown as a gray line and is based on the spectral analysis of 1000 simulations of red noise, using the Monte-Carlo algorithm. In the right hand side figures, the wavelet power spectrum is shown for each of the time series (a), (b) and (c). The averaged period and standard deviation is shown at the left corner of each wavelet power spectrum. The characteristic periods obtained through the wavelet analysis by connecting maximums of power spectrum per day are shown in (d).

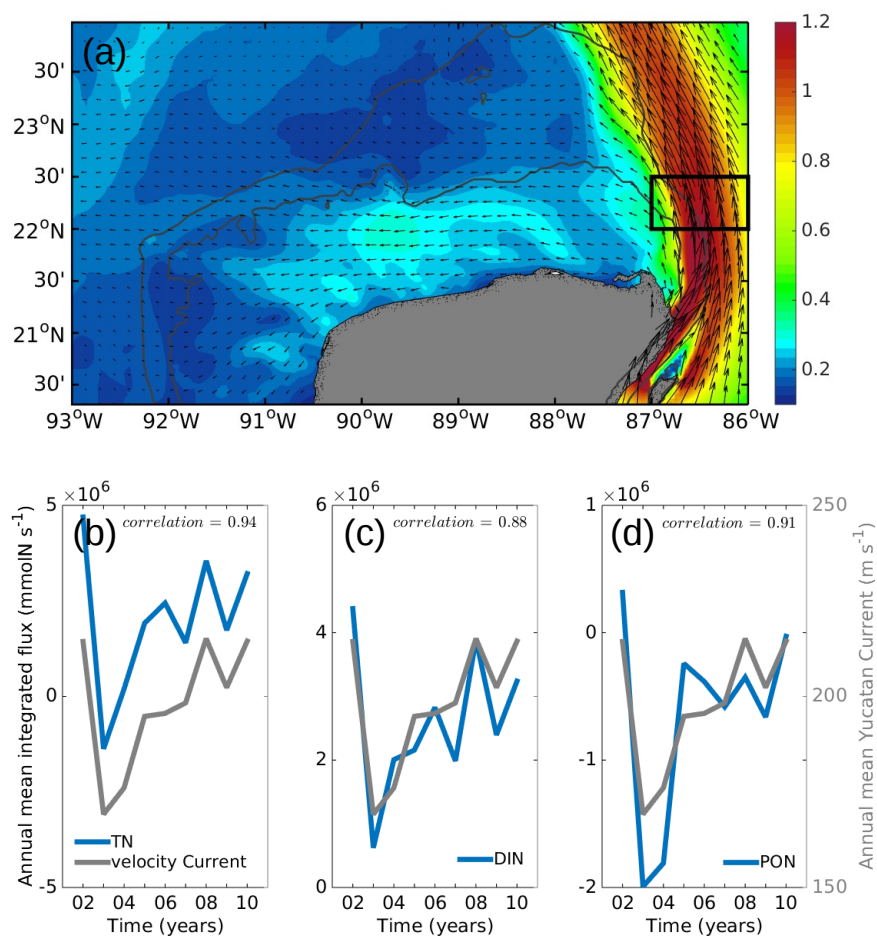


Figure 13. (a) Map of the annual mean surface velocity current for the year 2003. Vectors represent the direction of the flux and the two 50 m and 250 m isobath are shown. Correlation of the annual mean surface velocity current, averaged in the black box denoted in (a), with the annual mean of the integrated nitrogen fluxes at the East outer shelf margin for the 10 years of (b) the Total Nitrogen (TN), (c) the Dissolved Inorganic Nitrogen (DIN) and (d) the Particulate Organic Nitrogen (PON). The correlation values are shown at the right upper corner.

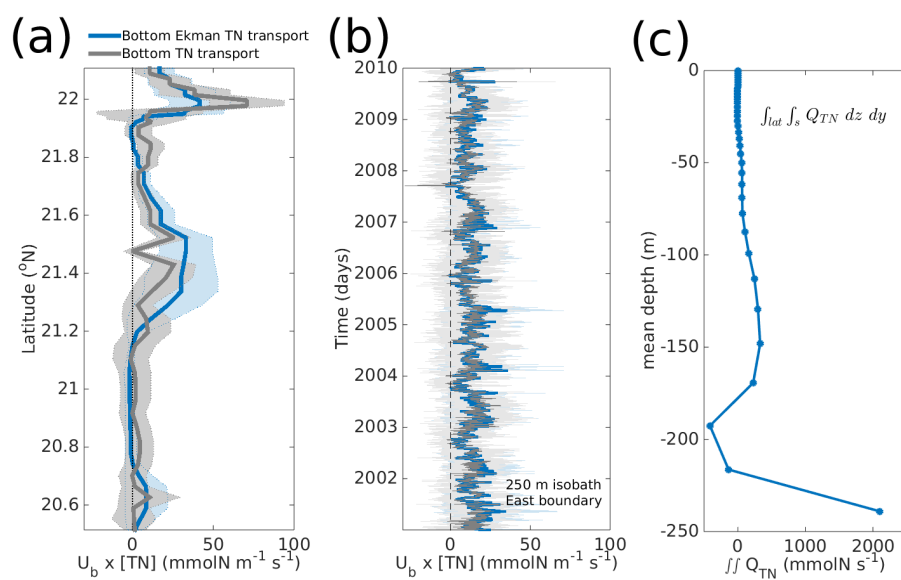


Figure 14. Flux of total nitrogen (TN) computed by the Bottom Ekman transport (U_{bE} , $\text{m}^2 \text{s}^{-1}$) for the nine simulated years (blue) compared with the bottom-most layer TN flux (gray) over the Ekman bottom layer for: (a) temporal averages and (b) spatial averages over the 250 m isobath. Shaded areas denote the standard deviation of the averages. (c) Doubled spatial integrated TN flux along the eastern 250 m isobath, over latitude and over s-layers. The TN flux is first averaged over the nine simulated years.

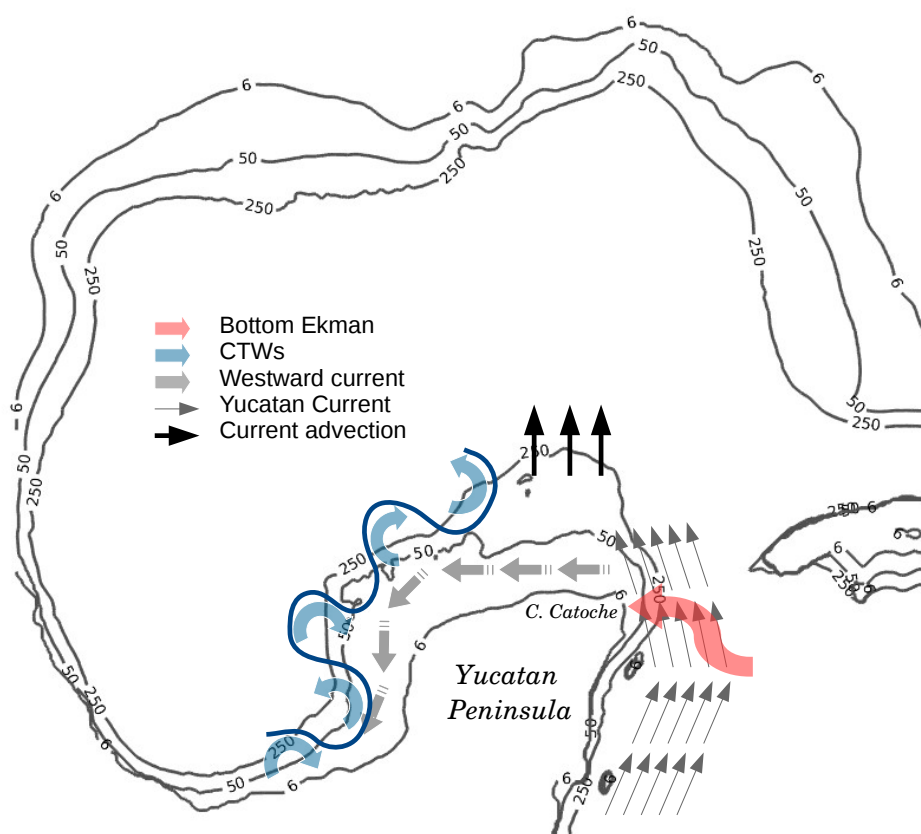


Figure 15. Schematic view of the main physical processes that modulate the cross-shelf transport of TN in the Yucatan shelf.

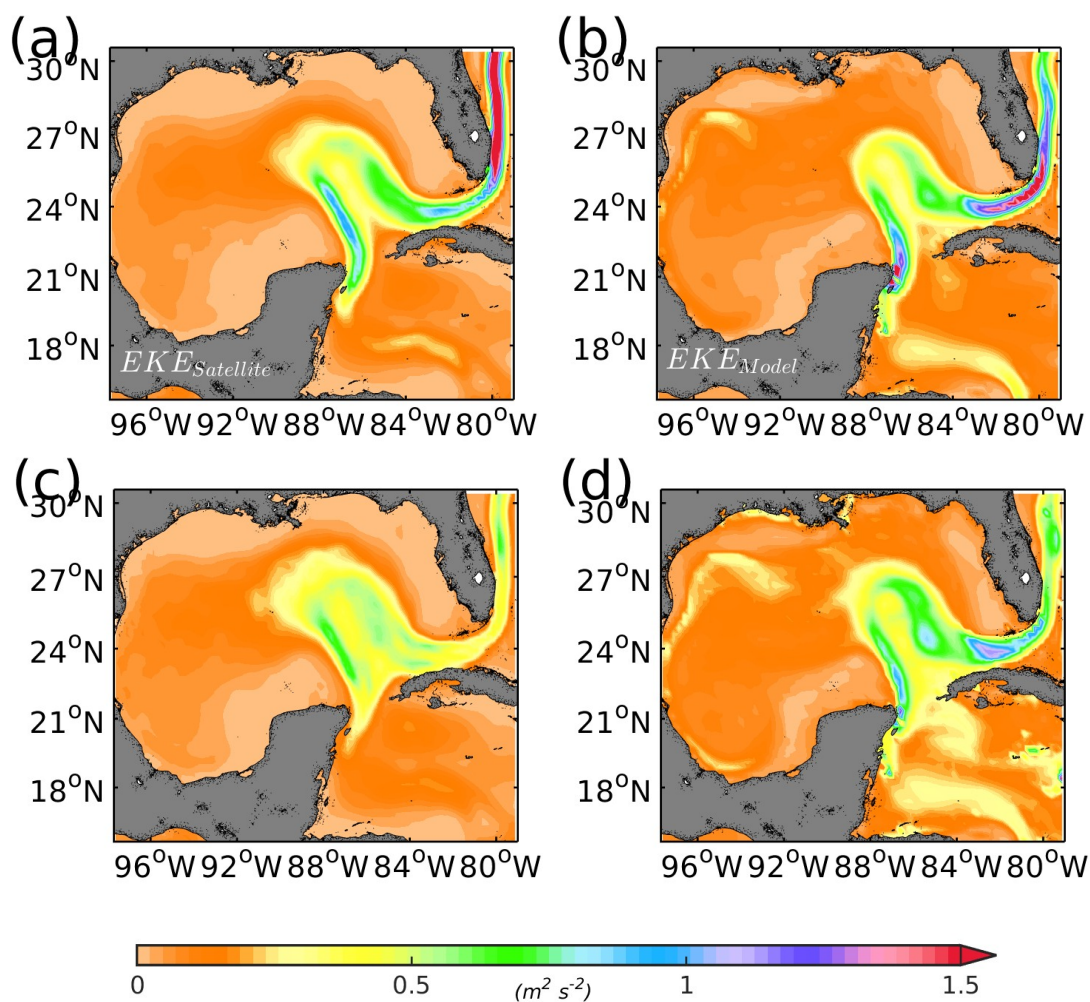


Figure A1. Comparison of 17 yr (1995-2012) averaged Eddy Kinetic Energy (EKE, $m^2 s^{-2}$) calculated in base on (a) AVISO SSH product and (b) ROMS model simulated SSH. (c) and (d) are the standard deviation for altimeter and model EKE, respectively.

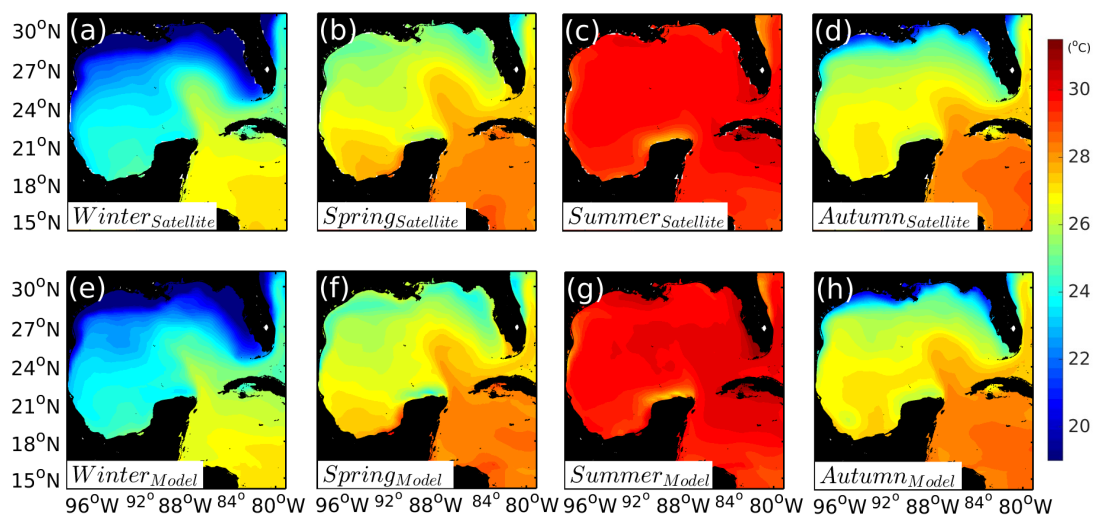


Figure A2. Seasonal climatologies of SST ($^{\circ}C$) for the GoM (2005 to 2012). Comparison between (a-d) satellital SST product and (e-h) model SST.

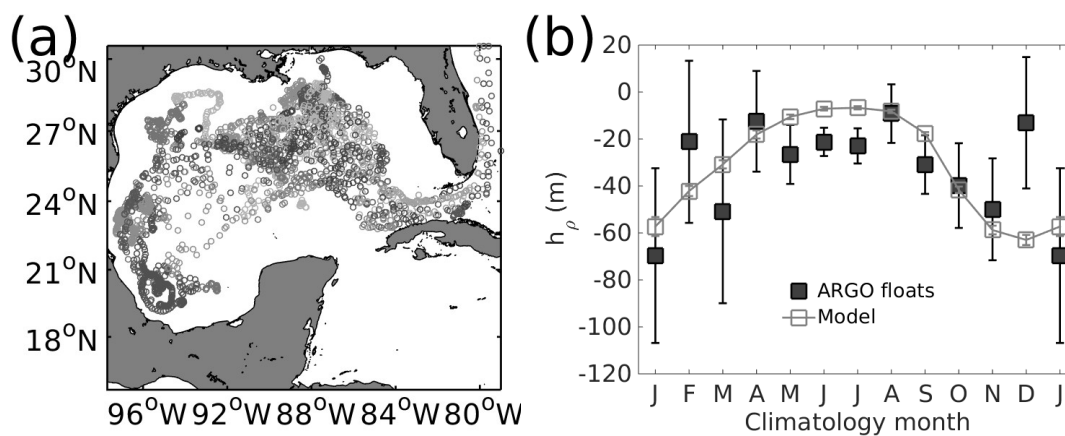


Figure A3. (a) Location of the 2629 ARGO profiles used for compute the mixed layer depth (h_p , m). (b) Climatology comparison of mixed layer depths for ARGO profile floats (black boxes) and for the model (gray boxes). Vertical lines in the boxes denote standard deviation.